consent, and (3) the presence of another known malignancy. Fifteen patients were excluded for the following reasons: 5 had contraindications to MRI because of claustrophobia, pacemaker, or prosthesis; 2 were unable to undergo SPIO because of hepatic insufficiency; 3 were unable to provide informed consent; and 5 had another malignancy (3 colorectal cancer, 1 gastric cancer, and 1 breast cancer). The remaining of 92 patients underwent hepatic SPIO-enhanced MR imaging for screening metastases from pancreatic cancer. The diagnosis of pancreatic cancer was confirmed by histologic findings of surgically resected specimens or surgically performed biopsies in 43 patients, cytologic findings of samples collected in endoscopy examinations in 35 patients, and the clinical courses and typical image findings in the remaining 14 patients. Ten patients were excluded for the following reasons: final diagnosis not established (n = 3), or the presence of more than 10 hepatic lesions (n = 7). Therefore, data for 82 patients (mean age, 55 years; range, 32–85 years), including 43 males (mean age, 52 years; range, 32–78 years) and 39 females (mean age, 58 years; range, 36–85 years), were analyzed in the study.

Eligibility of hepatic metastases from pancreatic cancer was obtained as follows. First, hepatic metastases from pancreatic cancer were pathologically diagnosed. If surgery was not performed, the hepatic lesions were diagnosed by the interval growth on images and clinical courses. Hepatic lesions were excluded if they were not pathologically diagnosed post operation or proved difficult to diagnose from the interval evaluation or clinical courses.

MR Image Acquisition and Preparation

The patients underwent upper abdominal MRI examinations using a 1.5-T system (Magnetom Symphony; Siemens Medical Systems, Erlangen, Germany) equipped with a six-channel body phased-array coil. MR imaging with different image contrasts was performed and grouped into (A) to (E), as specified below (summarized in Table 1). Before administration of SPIO (Resovist; Bayer Schering Pharma, Osaka, Japan), fat-saturated T2-weighted TSE imaging, and T1-weighted gradient-echo GRE imaging with dual-echo of in- and opposed-phases were acquired and grouped in the basic image set (A), which was also included in the other image sets from (B) to (E). For the basic image set (A), fat-saturated T2-weighted TSE imaging was conducted with the following parameters: repetition time/echo time (TR/TE), 5330/103 milliseconds; echo train length (ETL), 29; echo train spacing (ETS), 6.4 milliseconds; matrix size, 154 × 256; number of slices, 24; acquisition time, 27 seconds during 2 separate breath-holds at end-expiration. T1-weighted GRE imaging was performed with the following parameters: TR/TE in-phase/TE opposed-phase, 204/4.8/2.4 milliseconds; flip angle (FA), 80 degrees; matrix size, 195 × 256; number of slices, 24; acquisition time, 17 seconds during a breath-hold at end-expiration. Subsequently, diffusion-weighted imaging was conducted with respiration triggering using the prospective acquisition correction (PACE) method before SPIO administration and assigned to image set (B). The parameters were as follows: TR/TE, 1780–3220/91 milliseconds; b factors, 0, 500, and 1000 seconds/mm^2; generalized auto-calibrating partially parallel acquisition (GRAPPA) factor, 2; matrix size, 106 × 128; number of slices, 30; average acquisition time, 173 ± 33 seconds in average.

TABLE 1. Sequences of the 5 MR Image Sets

Sequences	Image Sets A	B	C	D	E
Non-SPIO-enhanced sequences					
T1-weighted GRE (in-phase and opposed-phase)	○	○	○	○	○
Fat-saturated T2-weighted TSE	○	○	○	○	○
Diffusion-weighted imaging*		○			
SPIO-enhanced sequences					
Fat-saturated T2-weighted TSE without PROPELLER*			○		
T2*-weighted GRE				○	
Fat-saturated T2-weighted TSE with PROPELLER*					○

The sequences used for imaging sets are indicated with circles. *Diffusion-weighted imaging and fat-saturated T2-weighted TSE imaging with and without PROPELLER were conducted with PACE. SPIO indicates super-paramagnetic iron oxide; GRE, gradient echo; TSE, turbo spin echo; PACE, prospective acquisition correction; PROPELLER, periodically rotated overlapping parallel lines with enhanced reconstruction.

After the acquisition of image sets (A) and (B), SPIO was administered at a dose of 0.016 mL [8 μmol of iron] per kilogram body weight (maximum: 1.4 mL), which was immediately followed by a saline flush. Over 10 minutes after injection, fat-saturated T2-weighted TSE imaging, T2*-weighted GRE imaging, and fat-saturated T2-weighted TSE imaging with the PROPELLER method were conducted and assigned to image sets of (C), (D), and (E), respectively. For image set (C), fat-saturated T2-weighted TSE imaging was performed under respiration triggering using PACE with the following parameters: TR/TE, 3448–6889/85 milliseconds; ETL, 31; ETS, 5.3 milliseconds; matrix size, 256 × 256; number of slices, 27; average acquisition time, 234 ± 47 seconds in average. For image set (D), T2*-weighted GRE images were acquired first with the following parameters: TR/TE, 169/9 milliseconds; FA, 60 degrees; matrix size, 179 × 256 with reduced field-of-view in the former direction by 80%[8]; number of slices, 24; acquisition time, 48 seconds during 2 separate breath-holds at end-expiration. For image set (E), fat-saturated T2-weighted images were acquired with both PROPELLER and PACE methods with the following parameters: TR/TE, 3462–6766/85 milliseconds; ETL, 31; ETS, 5.3 milliseconds; number of blades, 14; matrix size, 256 × 256; number of slices, 27; average acquisition time, 305 ± 58 seconds. All imaging covered the whole liver with transverse slices of 6 mm thickness with a gap of 1 mm in most cases. Slice thickness, slice gap and field of view were occasionally modified, dependent on the size of the body and the liver, but they were changed in all sequences compared and the effect of changing them is shared among all sequences. The order of sequences was conducted randomly among pre or postcontrast MR imagings.

Image Data Analysis

One abdominal radiologist (Y.H.; with 13 years of experience) removed any information related to the patient or examination method to avoid giving bias to evaluators. He did not participate in the data analysis. He attended the assessment and presented all image data sets (5 image sets for 82 patients) in a randomized order to evaluators, who were blinded to the aforementioned information. Any 2 image sets from a subject was presented at intervals of more than 4 weeks to minimize possible case memorization. All images sets were presented at random and were evaluated independently by 3 experienced abdominal radiologists (H.I., S.A., and K.S.; with 21, 9, and 9 years of experience, respectively) with a Digital Imaging and Communications in Medicine viewer (Centricity, version 2.0; GE Healthcare BioSciences, Tokyo, Japan). Each evaluator independently checked the presence of hepatic lesions on the basis of a 5-point confidence scale: 1, definitely or almost definitely absent; 2, probably absent; 3, possibly present; 4, probably present; and 5, definitely or almost definitely present. The evaluators also noted the segments in which they founded the suspected hepatic lesions. If

they found multiple lesions in one section level, all suspected lesions were scored individually.

To evaluate the image sets, the basic image set (A) was used to detect a nonsolid hepatic lesion, which was observed as an area of low intensity on the T1-weighted image and as high and homogenous signal intensity, similar to that of fluid components, such as cerebrospinal fluid, on fat-saturated T2-weighted TSE images. After exclusion of nonsolid hepatic lesions, hepatic metastases were defined as solid nodules showing higher signal intensity than hepatic parenchyma on precontrast T2-weighted images in image set (A), diffusion-weighted images in (B), or postcontrast T2 or T2*-weighted images in (C) to (E). These criteria were presented as a reference to the evaluators, and the final decision was at the discretion of each reader.

Statistical Analysis

Based on the reviews of the 3 observers, an alternative free-response receiver operating characteristic (ROC) analysis was performed to evaluate the detection of all hepatic lesions. For each image set, an alternative free-response ROC curve was fitted to each evaluator's confidence rating using a maximum likelihood estimation program (ROCKIT 1.0.1 B2; Metz CE, University of Chicago, IL, 1998). The diagnostic accuracy of each image set for each observer and the composite data were calculated by measuring the area under the alternative free-response ROC curve (A_z). The relative sensitivity of detection was calculated for lesions allocated a rating of 4 or 5. The differences between image sets in terms of the mean A_z were analyzed with Bonferroni method for post hoc analysis when the overall differences determined by the repeated-measures analysis of variance were assessed considering a normal distribution. The sensitivity for the detection of hepatic metastases (on a per-lesion basis) and the positive predictive value for each image set were also calculated. Size-wise analyses of the lesions were conducted for all sizes of lesions, those larger than 1 cm, and those 1cm or smaller.[8] Lesions were categorized by size based on the final reference (ie, histopathologic findings, intraoperative ultrasonography, or preoperative images if an operation was not conducted). This was followed by a statistical comparison of sensitivity by means of the McNemar test.

To assess interobserver variability in interpreting images, κ statistics were calculated to measure the degree of agreement; κ values of 0.00 implied poor agreement; 0.01 to 0.20, slight agreement; 0.21 to 0.40, fair agreement; 0.41 to 0.60, moderate agreement; 0.61 to 0.80, substantial agreement; and 0.81 to 1.0, almost perfect agreement. A P value less than 0.05 was considered to indicate a statistically significant difference. All statistical analyses were performed using SPSS statistical software (SPSS version 15.0, SPSS Inc., Chicago, IL).

RESULTS

All MR examinations were completed successfully without any adverse effects.

Hepatic Lesions

There were 72 nonsolid lesions (54 cysts and 18 hemangiomas). Fifty-one nonsolid (36 cysts and 15 hemangiomas) lesions were diagnosed based on the characteristic findings of contrast-enhanced CT, gadolinium-enhanced MR imaging, or ultrasonography, and the other 21 lesions (18 cysts and 3 hemangiomas) were pathologically confirmed at resection. Of the 82 eligible patients, after exclusion of these nonsolid lesions, 38 patients had a total of 111 focal hepatic metastatic lesions, and 44 patients had no focal hepatic lesions in the total of 82 patients. Of the 111 metastatic lesions, 45 hepatic metastatic lesions (28 lesions larger than 1 cm, 17 lesions 1 cm or smaller) in 20 patients were pathologically confirmed by surgical resections or biopsies. The remaining 57 hepatic lesions (29 lesions larger than 1 cm, 28 lesions 1 cm or smaller) in 11 patients were nonpathologically diagnosed based on the interval growth on follow-up images and on clinical courses. Nine lesions in 7 patients were excluded because of the following reasons: 2 lesions (both smaller than 1 cm) in 2 patients could not be pathologically confirmed using the excised specimen; 7 lesions (3 lesions larger than 1 cm, 4 lesions 1 cm or smaller) in 5 patients proved difficult to diagnose based on interval evaluation or clinical courses. Therefore, a total of 102 focal hepatic metastatic lesions in 31 patients were evaluated. Fifty-seven lesions were larger than 1 cm, and 45 lesions were 1 cm or smaller (mean size, 1.6 cm; range, 0.3–3.3 cm). The maximum number of malignant lesions in any patient was 7.

Interobserver Variability

The κ values for the 3 evaluators are summarized in Table 2. The analysis of interobserver agreement for all lesion groups and modalities indicated moderate to almost perfect agreements, and was very high in image set (E). Thus, the mean values were used for the analysis of accuracy (A_z) and pooled values were used for sensitivity and positive predictive values.

Accuracy

The mean A_z values obtained for the evaluation of hepatic lesions are presented in Table 3. The A_z values for image sets (B) to (E) were significantly greater than those for the basic image set (A) ($P < 0.001$). For the other MR image sets, (C) had the smallest values ($P < 0.001$) and (E) had the largest values, which were significantly larger than the others sets, including (B), ie, diffusion weighted imaging, irrespective of lesion size ($P < 0.001$). The nonenhanced image set (B) had similar values to those of (D) (n.s.).

Sensitivity

The pooled results for the sensitivity of detection of hepatic lesions for all 3 observers are summarized in Table 4. In the

TABLE 2. Level of Interobserver Agreement for the Detection of Hepatic Lesions

Lesion Sizes and Image Sets	Observers		
	1 vs. 2	2 vs. 3	1 vs. 3
All lesions			
A	0.65 ± 0.06	0.67 ± 0.07	0.64 ± 0.07
B	0.70 ± 0.06	0.71 ± 0.07	0.67 ± 0.06
C	0.68 ± 0.06	0.65 ± 0.07	0.70 ± 0.06
D	0.79 ± 0.05	0.75 ± 0.06	0.76 ± 0.05
E	0.82 ± 0.04	0.78 ± 0.05	0.81 ± 0.05
Lesions >1 cm			
A	0.68 ± 0.06	0.64 ± 0.07	0.65 ± 0.07
B	0.75 ± 0.05	0.76 ± 0.07	0.71 ± 0.05
C	0.71 ± 0.06	0.70 ± 0.07	0.73 ± 0.06
D	0.82 ± 0.05	0.78 ± 0.06	0.82 ± 0.05
E	0.85 ± 0.04	0.83 ± 0.05	0.83 ± 0.05
Lesions ≤1 cm			
A	0.63 ± 0.07	0.70 ± 0.07	0.62 ± 0.08
B	0.62 ± 0.06	0.65 ± 0.08	0.63 ± 0.08
C	0.64 ± 0.06	0.62 ± 0.07	0.65 ± 0.05
D	0.73 ± 0.05	0.70 ± 0.07	0.68 ± 0.06
E	0.77 ± 0.05	0.73 ± 0.05	0.79 ± 0.04

See Table 1 for a description of the image sets. Data are κ values ± standard errors of the mean. The total sample size was 102 lesions (lesions >1 cm were, n = 57; ≤1 cm, n = 45) in 31 patients.

TABLE 3. Areas Under the Receiver Operating Characteristic Curves (A_z Values) for the Detection of Hepatic Lesions

	Lesion Size		
Image Sets	**All (n = 102)**	**>1 cm (n = 57)**	**≤1 cm (n = 45)**
A	0.58 ± 0.05	0.62 ± 0.05	0.53 ± 0.05
B	0.81 ± 0.04*†	0.86 ± 0.04*†	0.76 ± 0.05*†
C	0.70 ± 0.05*	0.76 ± 0.06*	0.61 ± 0.05*
D	0.80 ± 0.04*†	0.84 ± 0.04*†	0.73 ± 0.05*†
E	0.90 ± 0.03*‡†§	0.93 ± 0.03*‡†§	0.87 ± 0.03*‡†§

See Table 1 for a description of the image sets. Data are mean Az values ± standard errors of the mean.

Significantly higher ($P < 0.05$) than image sets *A, ‡B, †C, and §D.

TABLE 4. Sensitivity for the Detection of Hepatic Lesions

Lesion Sizes and Image Sets	Sensitivity	95% CI	*P*
All lesions			
A	0.47 (145/306)	42, 53	
B	0.69 (211/306)	63, 74	*†
C	0.56 (172/306)	50, 62	*
D	0.66 (201/306)	60, 71	*†
E	0.77 (235/306)	72, 81	*†‡§
Lesions >1 cm			
A	0.51 (88/171)	44, 59	
B	0.73 (125/171)	66, 80	*†
C	0.60 (103/171)	52, 68	
D	0.71 (122/171)	64, 78	*†
E	0.81 (139/171)	75, 87	*†
Lesions ≤1 cm			
A	0.42 (57/135)	34, 51	
B	0.64 (86/135)	55, 72	*†
C	0.51 (69/135)	42, 60	
D	0.59 (79/135)	50, 67	*
E	0.71 (96/135)	63, 79	*†§

See Table 1 for a description of image sets. The total sample size was 102 lesions (lesions >1 cm, n = 57; ≤1 cm, n = 45) in 31 patients. Data are percentages. Data in parentheses were those used to calculate the sensitivity values. *P* values were calculated with the McNemar test.

Significantly higher ($P < 0.05$) than image sets *A, ‡B, †C, and §D.

CI indicates confidence interval.

all-lesion group, the sensitivity of image sets (B) to (E) was higher than that of the basic image set (A). Image set (E) had the highest sensitivity and was significant higher than the other image sets, including (B) ($P < 0.01$). Image sets (B) and (D) had comparable values (n.s.), which were significantly higher than those for (C) ($P < 0.01$). When classified by lesion size, similar patterns were observed, but some of the comparisons did not reach statistical significance, including the differences between (B) and (E) (Table 4).

Positive Predictive Value

The pooled positive predictive values for the detection of hepatic lesions are shown in Table 5. Irrespective of the lesion groups, the mean positive predictive values for the basic image set (A) were the lowest, followed by image set (C); those for image set (E) were the highest. The mean positive predictive values for image set (B) were lower than those for image set (D) for all lesions and for lesions 1 cm or smaller, whereas those for image set (B) were slightly higher than those for image set (D) for lesions larger than 1 cm.

TABLE 5. Positive Predictive Values for the Detection of Hepatic Lesions

Lesion Sizes and Image Sets	Positive Predictive Value	95% CI
All lesions		
A	0.76 (145/190)	70, 82
B	0.85 (211/247)	80, 90
C	0.81 (172/212)	75, 86
D	0.89 (201/226)	84, 93
E	0.94 (235/251)	90, 96
Lesions >1 cm		
A	0.81 (88/108)	73, 88
B	0.93 (125/134)	88, 97
C	0.85 (103/121)	78, 91
D	0.92 (122/132)	87, 96
E	0.95 (139/146)	90, 88
Lesions ≤1 cm		
A	0.70 (57/82)	58, 79
B	0.76 (86/113)	67, 84
C	0.76 (69/91)	66, 84
D	0.84 (79/94)	75, 91
E	0.91 (96/105)	84, 96

See Table 1 for a description of the image sets. The total sample size was 102 lesions (lesions >1 cm, n = 57; ≤1 cm, n = 45) in 31 patients. Data are percentages. Data in parentheses were those used to calculate the positive predictive values.

CI indicates confidence interval.

The majority of false-positive lesions were blurring and motion artifacts such as physical movement, respiratory motion (Fig. 1) and cardiovascular pulsation (Fig. 2), benign lesions (ie, bile duct adenoma, biliary hamartoma, hemangioma), and partial volume effect of hepatic tissue. MR image set (B) had relative lower values for lesions 1 cm or smaller than the other enhanced sequences, in contrast with the sensitivity results.

False-Negative Findings

At the confidence levels of 4 or 5, 16 lesions in 12 patients were not detected by any observer for any image sets. Of these 16 lesions, in 6 patients, 10 lesions were smaller than 1 cm (six, <5 mm). For image set (E) alone, 12 lesions (seven ≤1 cm) in 8 patients could be detected by at least one observer. Four lesions (three <1 cm) in 3 patients were observed by at least one observer with (B) alone and 2 lesions (one <1 cm) in 2 patients could be observed with (D) alone. With regard to false-negative lesions, blurring and motion artifacts were responsible for degrading image quality.

DISCUSSION

SPIO-enhanced MR imaging has been used to improve the detection and characterization of hepatic lesions. Gadolinium ethoxybenzyl diethylenetriaminepentaacetic acid (Gd-EOB-DTPA), a gadolinium-based contrast agent that targets hepatocytes, was reported to be an effective method for the detection of colorectal liver metastasis[22] and is currently under intensive investigation. Gadobenate dimeglumine (Gd-BOPTA)-enhanced delayed-phase imaging was also reported to have comparable diagnostic performance to SPIO-enhanced imaging for the detection of liver metastases, and had a better diagnostic performance than Gd-BOPTA-enhanced dynamic images in patients with liver metastasis.[23] However, another study showed that, when Gd-BOPTA-enhanced MR imaging was compared with SPIO-enhanced MR imaging, only

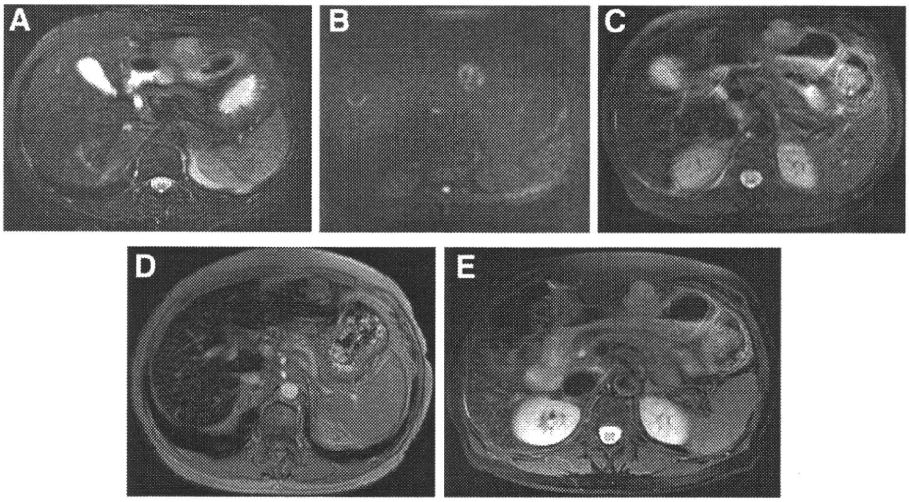

FIGURE 1. Images obtained using superparamagnetic iron oxide-enhanced (SPIO) administration obtained in a 55-year-old woman with hepatic metastasis from pancreatic cancer. Precontrast (A) fat-saturated T2-weighted TSE (5330/103), and (B) diffusion-weighted GRAPPA (2100/91; b-factor, 1000 seconds/mm^2) MR images. Postcontrast (C) fat-saturated T2-weighted TSE with respiratory triggering (PACE), (D) T2*-weighted GRE (169/9, 60 degrees flip angle), and (E) fat-saturated PROPELLER T2-weighted TSE with PACE MR images. A 3-cm diameter metastasis is seen in the lateral segment of the left lobe on all images. The patient is moving during the MR examination, and the hepatic lesion is the most clearly seen and given the best motion correction on the PROPELLER MR image (E). Some differences in slice position are observed because of respiration, although images were planned for the same position. Note that the hyperintense lesions in the right lobe (A, B, D) and in segment IV (C) were confirmed to be pseudo-lesions.

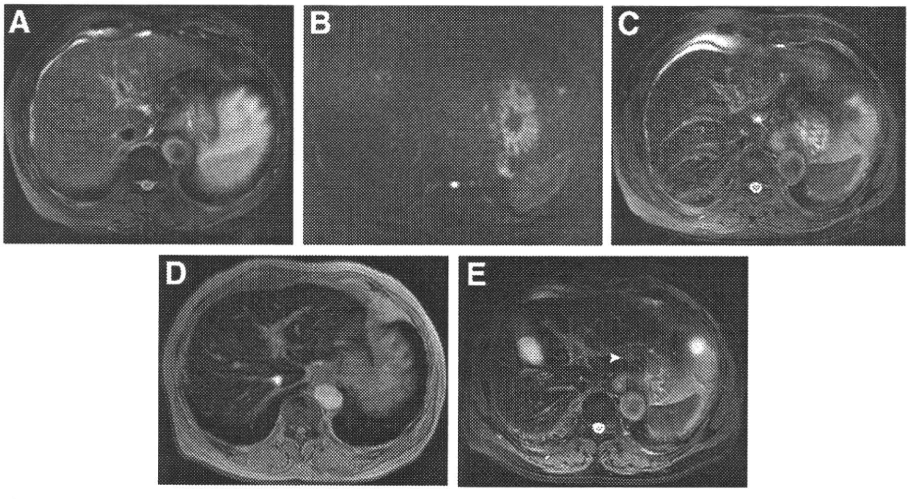

FIGURE 2. Abdominal images obtained using superparamagnetic iron oxide-enhanced (SPIO) administration in a 48-year-old man with pancreatic cancer. Precontrast (A) fat-saturated T2-weighted TSE (5330/103) and (B) diffusion-weighted GRAPPA (2100/91; b-factor, 1000 seconds/mm^2) MR images. Postcontrast (C) fat-saturated T2-weighted TSE with respiratory triggering (PACE), (D) T2*-weighted GRE (169/9, 60 degrees flip angle) and (E) fat-saturated PROPELLER T2-weighted TSE with PACE MR images. The hepatic metastatic lesion is obscure in all images except for that with the PROPELLER sequence (E) because of image artifacts. The 0.9-cm diameter hepatic tumor (arrowhead) in segment II can only be clearly observed using the PROPELLER method (E). Note that the hyperintense subcapsular lesions in segment IV (A, B) and in the right lobe (C, D) were confirmed to be pseudolesions.

SPIO-enhanced MRI was found to able to detect all liver metastases of less than 1 cm and was recommended for diagnosis of small colorectal liver metastases.[24] Therefore, improvements in SPIO-enhanced MRI remain an important technical issue. Hence, some physicians believe that SPIO-enhanced MR imaging is one of the most appropriate preoperative imaging procedures for the screening of hepatic metastases and shows high ability to differentiate between benign and malignant focal liver lesions on the basis of their cellular composition and function.[25] SPIO-enhanced MR imaging can be conducted in patients with advanced kidney disease who may develop nephrogenic systemic fibrosis as a result of gadolinium toxicity.[26,27]

Although various pulse sequences have been used by many investigators for SPIO-enhanced MR imaging, T2*-weighted GRE

sequences are regarded as an essential method to detect focal hepatic lesions.[25,28,29] A previous study reported that respiratory-triggered T2-weighted TSE images after SPIO administration provided greater tumor-to-liver contrast and subjective conspicuity for hepatic lesions.[30] However, motion artifacts caused by respiration, cardiovascular pulsation, peristalsis, and physical movement deteriorate abdominal MR image quality and prevented lesion detection.[31–33] To overcome these limitations, a recently introduced acquisition technique PROPELLER can be used instead. It has a theoretical advantage of central k-space oversampling,[11] which was reported to reduce motion-related image artifacts[20] as well as increase SNR[21] in clinical cases. The PROPELLER technique applied to the upper abdominal imaging improved the quality of T2-weighted TSE imaging.[10,18–21] Therefore, it was reasonable to hypothesize that fat-saturated T2-weighted TSE imaging with the PROPELLER technique in combination with SPIO administration may improve the detection of hepatic lesions compared with other sequences including diffusion-weighted imaging or SPIO-enhanced T2*-weighted GRE imaging.

The results of our study showed that the detection of hepatic lesions with the PROPELLER technique was superior to those with other sequences. In a previous study, MR imaging using the PROPELLER technique was shown to reduce image artifacts and image noise, resulting in better image quality in the upper abdomen.[18] This suggested the probability of improving the detection of hepatic lesions by adopting these methods. With the use of SPIO-enhanced sequences, the accuracy and sensitivity for the detection of hepatic lesions were higher than those of the unenhanced basic image set. Notably, the SPIO-enhanced MR sets using the T2*-weighted GRE sequence obtained during breath-hold was statistically better than fat-saturated T2-weighted TSE with PACE. This might be due to image artifacts caused by a mismatch in the respiratory rhythm or by and increased magnetization transfer saturation.[34,35] On the other hand, T2*-weighted GRE imaging may be affected by low SNR and susceptible artifacts.[36] The PROPELLER technique can offer motion correction to overcome these limitations.[37,38] About half of the hepatic metastases in the current study were equal to or smaller than 1 cm in size, and fat-saturated T2-weighted TSE imaging with PROPELLER was confirmed to show the highest sensitivity for these metastases.

Several reports showed the high ability for body diffusion-weighted images to detect various malignant tumors.[8,39–42] Diffusion-weighted MR imaging using high-b-value achieved detection of colorectal, pancreatic adenocarcinoma and focal liver masses with high sensitivity and specificity.[39,40,42] Combined reading of diffusion-weighted images and unenhanced T1/T2-weighted images (ie, the basic image set) had higher accuracy for the detection of hepatic metastases than SPIO-enhanced MR images.[8] In the present study, SPIO-enhanced MR sets using PROPELLER technique enabled improved detection of hepatic lesions 1 cm in diameter or smaller as well as lesions larger than 1 cm than the MR sets using diffusion-weighted images. There were some false-positive and false-negative lesions on the MR sets using diffusion-weighted images because of distortion and misregistration of fat tissue, image artifacts, and low resolution after combined interpretation of fat-saturated T2-weighted TSE images. The PROPELLER technique might be useful to detect hepatic lesions affected by image artifacts such as respiratory motion, cardiovascular pulsation, bowel movement, and physical movement that deteriorate MR image quality. However, 4 lesions (3 lesions smaller than 1 cm) were only detectable in the diffusion-weighted images and it has a certain contribution to improvement of diagnostic capability.

There are several potential limitations in our study. First, not all of the hepatic lesions were pathologically confirmed. However, typical clinical and laboratory findings, in combination with disease progression in follow-up images, clearly indicated malignancy. Second, the image acquisition time increased with the PROPELLER technique. It may improve SNR, but also requires time for motion correction. The use of techniques such as parallel acquisition might reduce the acquisition time. Third, the parameters associated with PROPELLER acquisition, such as echo train length, blade width and number of blades, were not investigated in this study and may not be fully optimized. Therefore, we should investigate the optimal PROPELLER MR imaging parameters in future studies. Fourth, diffusion-weighted MR imaging in combination with the PROPELLER technique was not applicable because of limited abilities of the apparatus used here. Finally, no ADC analysis was conducted in this study; however, it could be misleading[43] and we did not use it.

In summary, SPIO-enhanced MR imaging with the PROPELLER technique is likely to improve the detection of hepatic metastases from pancreatic cancer in comparison with diffusion-weighted MR imaging, fat-saturated T2WI without PROPELLER technique, or SPIO-enhanced T2*-weighted GRE imaging. Further clinical studies are required to evaluate abdominal MR imaging with the use of optimized PROPELLER methods.

REFERENCES

1. Bartolozzi C, Lencioni R, Donati F, et al. Abdominal MR: liver and pancreas. *Eur Radiol.* 1999;9:1496–1512.
2. Bartolozzi C, Cioni D, Donati F, et al. Focal liver lesions: MR imaging-pathologic correlation. *Eur Radiol.* 2001;11:1374–1388.
3. Kondo H, Kanematsu M, Hoshi H, et al. Preoperative detection of malignant hepatic tumors: comparison of combined methods of MR imaging with combined methods of CT. *Am J Roentgenol.* 2000;174:947–957.
4. Coenegrachts K, Orlent HO, ter Beek L, et al. Improved focal liver lesion detection: comparison of single-shot spin-echo echo-planar and superparamagnetic iron oxide (SPIO)-enhanced MRI. *J Magn Reson Imaging.* 2008; 27:117–124.
5. Soyer P, Levesque M, Caudron A, et al. MRI of liver metastases from colorectal cancer vs. CT during arterial portography. *J Comput Assist Tomogr.* 1993;17:67–74.
6. Heiken JP, Weyman PJ, Lee JK, et al. Detection of focal hepatic masses: prospective evaluation with CT, delayed CT, CT during arterial portography, and MR imaging. *Radiology.* 1989;171:47–51.
7. Semelka RC, Schlund JF, Molina PL, et al. Malignant liver lesions: comparison of spiral CT arterial portography and MR imaging for diagnostic accuracy, cost, and effect on patient management. *J Magn Reson Imaging.* 1996;1:39–43.
8. Nasu K, Kuroki Y, Nawano S, et al. Hepatic metastases: diffusion-weighted sensitivity-encoding versus SPIO-enhanced MR imaging. *Radiology.* 2006; 239:122–130.
9. Chow LC, Bammer R, Moseley ME, et al. Single breath-hold diffusion-weighted imaging of the abdomen. *J Magn Reson Imaging.* 2003;18:377–382.
10. Deng J, Miller FH, Salem R, et al. Multishot diffusion-weighted PROPELLER magnetic resonance imaging of the abdomen. *Invest Radiol.* 2006;41: 769–775.
11. Pipe JG. Motion correction with PROPELLER MRI: application to head motion and free-breathing cardiac imaging. *Magn Reson Med.* 1999;42:963–969.
12. Wintersperger BJ, Runge VM, Biswas J, et al. Brain magnetic resonance imaging at 3 Tesla using BLADE compared with standard rectilinear data sampling. *Invest Radiol.* 2006;41:586–592.
13. Fobes KP, Pipe JG, Bird CR, et al. PROPELLER MRI: clinical testing of a novel technique for quantification and compensation of head motion. *J Magn Reson Imaging.* 2001;14:215–222.
14. Fobes KP, Pipe JG, Karis JP, et al. Improved image quality and detection of acute cerebral infarction with PROPELLER diffusion-weighted MR imaging. *Radiology.* 2002;225:551–555.
15. Attenberger UI, Runge VM, Stemmer A, et al. Diffusion Weighted Imaging: A Comprehensive Evaluation of a Fast Spin Echo DWI Sequence With

BLADE (PROPELLER) k-Space Sampling at 3 T, Using a 32-Channel Head Coil in Acute Brain Ischemia. *Invest Radiol.* 2009;44:656–661.

16. Attenberger UI, Runge VM, Williams KD, et al. T1-Weighted Brain Imaging With a 32-Channel Coil at 3T Using TurboFLASH BLADE Compared With Standard Cartesian k-Space Sampling. *Invest Radiol.* 2009;44:177–183.
17. Deng J, Larson AC. Multishot targeted PROPELLER magnetic resonance imaging: description of the technique and initial applications. *Invest Radiol.* 2009;44:454–462.
18. Kiryu S, Watanabe M, Kabasawa H, et al. Evaluation of super paramagnetic iron oxide-enhanced diffusion-weighted PROPELLER T2-fast spin echo magnetic resonance imaging: preliminary experience. *J Comput Assist Tomogr.* 2006;30:197–200.
19. Hirokawa Y, Isoda H, Maetani Y, et al. MRI artifact reduction and quality improvement in the upper abdomen with the PROPELLER (BLADE) and navigator triggered prospective acquisition correction (PACE) technique. *Am J Roentgenol.* 2008;191:1154–1158.
20. Hirokawa Y, Isoda H, Maetani Y, et al. Evaluation of motion correction effect and image quality with the periodically rotated overlapping parallel lines with enhanced reconstruction (PROPELLER) (BLADE) and parallel imaging acquisition technique in the upper abdomen. *J Magn Reson Imaging.* 2008; 28:957–962.
21. Hirokawa Y, Isoda H, Maetani Y, et al. Hepatic lesions: improved image quality and detection with the periodically rotated overlapping parallel lines with enhanced reconstruction technique—evaluation of SPIO-enhanced T2-weighted MR images. *Radiology.* 2009;251:388–397.
22. Zech CJ, Grazioli L, Jonas E, et al. Health-economic evaluation of three imaging strategies in patients with suspected colorectal liver metastases: Gd-EOB-DTPA-enhanced MRI vs. extracellular contrast media-enhanced MRI and 3-phase MDCT in Germany, Italy and Sweden. *Eur Radiol.* 2009;19(suppl 3):S753–S763.
23. Kim YK, Lee JM, Kim CS, et al. Detection of liver metastases: gadobenate dimeglumine-enhanced three-dimensional dynamic phases and one-hour delayed phase MR imaging versus superparamagnetic iron oxide-enhanced MR imaging. *Eur Radiol.* 2005;15:220–228.
24. Hekimoglu K, Ustundag Y, Dusak A, et al. Small colorectal liver metastases: detection with SPIO-enhanced MRI in comparison with gadobenate dimeglumine-enhanced MRI and CT imaging. *Eur J Radiol.* 2009;Sep 23. [Epub ahead of print].
25. Namkung S, Zech CJ, Helmberger T, et al. Superparamagnetic iron oxide (SPIO)-enhanced liver MRI with ferucarbotran: efficacy for characterization of focal liver lesions. *J Magn Reson Imaging.* 2007;25:755–765.
26. Cowper SE. Nephrogenic system fibrosis: the nosological and conceptual evolution of nephrogenic fibrosing dermopathy. *Am J Kidney Dis.* 2005;46: 763–765.
27. Perez-Rodriguez J, Lai S, Ehst BD, et al. Nephrogenic systemic fibrosis: incidence, associations, and effect of risk factor assessment—report of 33 cases. *Radiology.* 2009;250:371–377.
28. Kanematsu M, Ito K, Matsuo M, et al. Malignant hepatic tumor detection with ferumoxides-enhanced MR imaging with a 1.5-T system: comparison of four imaging pulse sequences. *J Magn Reson Imaging.* 2001;13:249–257.
29. Kim MJ, Kim JH, Choi JY, et al. Optimal TE for SPIO-enhanced gradient-recalled echo MRI for the detection of focal hepatic lesions. *Am J Roentgenol.* 2006;187:W255–W266.
30. Ishiyama K, Hashimoto M, Izumi J, et al. Tumor-liver contrast and subjective tumor conspicuity of respiratory-triggered T2-weighted fast spin-echo sequence compared with T2*-weighted gradient recalled-echo sequence for ferucarbotran-enhanced magnetic resonance imaging of hepatic malignant tumors. *J Magn Reson Imaging.* 2008;27:1322–1326.
31. Wood ML, Henkelmann RM. MR image artifacts from periodic motion. *Med Phys.* 1985;12:143–151.
32. Haacke EM, Patric JL. Reducing motion artifacts in two-dimensional Fourier transform imaging. *Magn Reson Imaging.* 1986;4:359–376.
33. Yang W, Smith MR. Using an MRI distortion transfer function to characterize the ghosts in motion-corrupted images. *IEEE Trans Med Imaging.* 2000;19: 577–584.
34. Abe Y, Yamashita Y, Namimoto T, et al. The value of fast and ultrafast T2-weighted MR imaging sequences in hepatic enhancement with ferumoxides: comparison with conventional spin-echo sequence. *Radiat Med.* 2000; 18:97–105.
35. Ward J, Guthrie JA, Wilson D, et al. Colorectal hepatic metastases: detection with SPIO-enhanced breath-hold MR imaging-comparison of optimized sequences. *Radiology.* 2003;228:709–718.
36. Abe Y, Yamashita Y, Namimoto T, et al. The value of fast and ultrafast T2-weighted MR imaging sequences in hepatic enhancement with ferumoxides: comparison with conventional spin-echo sequence. *Radiat Med.* 2000; 18:97–105.
37. Tanimoto A, Yuasa Y, Shinmoto H, et al. Superparamagnetic iron oxide-mediated hepatic signal intensity change in patients with and without cirrhosis: pulse sequence effects and Kupffer cell function. *Radiology.* 2002;222: 661–666.
38. Yoshikawa T, Mitchell DG, Hirota S, et al. Gradient- and Spin-echo T2-weighted imaging for SPIO-enhanced and characterization of focal liver lesions. *J Magn Reson Imaging.* 2006;27:712–719.
39. Ichikawa T, Erturk SM, Motosugi, et al. High-b-value diffusion-weighted MRI in colorectal cancer. *Am J Roentgenol.* 2006;187:181–184.
40. Ichikawa T, Erturk SM, Motosugi, et al. High-b-value diffusion-weighted MRI for detecting pancreatic adenocarcinoma. *Am J Roentgenol.* 2007;187: 409–414.
41. Tsushima Y, Takano A, Taketomi A, et al. Body diffusion-weighted MR imaging high b-value for malignant tumor screening: usefulness and necessity of referring to T2-weighted images and creating fusion imaging. *Acad Radiol.* 2007;14:643–650.
42. Erturk SM, Ichikawa T, Sano K, et al. Diffusion-weighted magnetic resonance imaging for characterization of focal liver masses: impact of parallel imaging (SENSE) and b value. *J Comput Assist Tomogr.* 2008;32:865–871.
43. Uto T, Takehara Y, Nakamura Y, et al. Higher sensitivity and specificity for diffusion-weighted imaging of malignant lung lesions without apparent diffusion coefficient quantification. *Radiology.* 2009;252:247–254.

European Journal of Radiology xxx (2009) xxx–xxx

Contents lists available at ScienceDirect

European Journal of Radiology

journal homepage: www.elsevier.com/locate/ejrad

The potential clinical value of FDG-PET for recurrent renal cell carcinoma

Koya Nakatani[a,*], Yuji Nakamoto[a,1], Tsuneo Saga[b,2], Tatsuya Higashi[c,3], Kaori Togashi[a,4]

[a] Department of Diagnostic Imaging and Nuclear Medicine, Kyoto University Graduate School of Medicine, 54 Shogoin-kawahara-cho, Sakyo-Ku, Kyoto 606-8507 Japan
[b] Department of Diagnostic Imaging Molecular Imaging Center, National Institute of Radiological Sciences, 4-9-1 Anagawa, Inage-Ku, Chiba 263-8555, Japan
[c] Research Institute, Shiga Medical Center for Adults, 5-4-30 Moriyama, Moriyama City, Shiga 524-8524 Japan

ARTICLE INFO

Article history:
Received 4 September 2009
Received in revised form
19 November 2009
Accepted 19 November 2009

Keywords:
^{18}F-FDG-PET
Renal cell carcinoma
Recurrence
Prognostic value

ABSTRACT

Purpose: The clinical value of positron emission tomography (PET) using ^{18}F-fluorodeoxyglucose (FDG) for follow-up or suspected recurrence of renal cell carcinoma (RCC) has not been fully evaluated. The purpose of this study was to assess the diagnostic performance of FDG-PET for postoperative assessment in patients with RCC.

Methods: We reviewed 28 scans in 23 patients who had undergone FDG-PET scans after surgery for RCC. Diagnostic accuracy of visually interpreted PET was evaluated based on final diagnoses obtained histologically or by clinical follow-up at least 6 months. Also, additional information over CT, influence on treatment decisions, and the accuracy of FDG uptake as a predictor of survival were assessed.

Results: Recurrence of renal carcinoma was histologically ($n = 15$) or clinically ($n = 6$) confirmed in 21 of 28 cases. Overall, the sensitivity, specificity, and diagnostic accuracy using FDG-PET were 81%, 71%, and 79%, respectively. In papillary RCC, the sensitivity was 100%; however, that was 75% in clear cell RCC in patient-basis. PET correctly detected local recurrence and metastases in all cases in the peritoneum, bone, muscle and adrenal gland. Additional information was obtained from scans in 6 cases (21%), which influenced therapeutic management in 3 cases (11%). Cumulative survival rates over 5 years in the PET-positive vs. the PET-negative group were 46% vs. 83%, respectively ($p = 0.17$).

Conclusions: FDG-PET would be useful for postoperative surveillance in patients with RCC, although its impact on treatment decisions may be limited. Further investigations are necessary to conclude whether PET has a prognostic value.

1. Introduction

Positron emission tomography (PET) with ^{18}F-fluorodeoxyglucose (FDG) has been widely used in clinical oncology as an established modality for imaging cancer. FDG-PET is applicable especially for staging or re-staging, and monitoring therapeutic response in several cancers. As for renal cell carcinoma (RCC), Wahl et al. reported the feasibility of metabolic imaging using FDG, as well as morphological imaging for primary and metastatic tumors in their pilot study in 1991 [1], followed by reports describing high accuracy of FDG-PET for the diagnosis of RCC [2–4]. Conversely, other reports have indicated higher false-negative rates [5,6]. Kang et al. examined 90 PET scans in 66 patients, and concluded that the role of FDG-PET in the detection of RCC was limited due to its low sensitivity and that, with superior specificity; PET might have a complementary role as a problem-solving tool in cases that were equivocal using conventional imaging [7]. Thus, the clinical role of FDG-PET for RCC remains controversial, but has not been considered helpful for the evaluation of primary RCC.

Meanwhile, the role of FDG-PET for follow-up or suspected recurrence of RCC has been reported to be favorable [8–10]. Clinical courses in patients with recurrent RCC following nephrectomy vary, with a survival benefit associated with sufficient metastasectomy [11–15]. More accurate diagnosis of recurrent RCC is important, but morphological imaging modalities, such as computed tomography (CT), have certain limitations for exact evaluation of recurrent RCC. Hence, metabolic imaging, including FDG-PET, is expected to demonstrate increased accuracy, but not much has been reported yet on the efficacy of PET in the diagnosis of recurrent RCC.

In the present study, to elucidate the clinical value of FDG-PET for recurrence and distant metastases of RCC, we assessed diagnostic performance of FDG-PET for postoperative survey in patients with RCC. Furthermore, we assessed whether FDG uptake could be a predictor of survival in patients with recurrent RCC.

* Corresponding author. Tel.: +81 75 751 3419; fax: +81 75 771 9709.
E-mail addresses: koyakn@kuhp.kyoto-u.ac.jp (K. Nakatani), 9709.ynakamo1@kuhp.kyoto-u.ac.jp (Y. Nakamoto), saga@nirs.go.jp (T. Saga), higashi@shigamed.jp (T. Higashi), ktogashi@kuhp.kyoto-u.ac.jp (K. Togashi).
[1] Tel.: +81 75 751 3762; fax: +81 75 771 9709.
[2] Tel.: +81 43 206 3429.
[3] Tel.: +81 77 582 6034; fax: +81 77 582 6041.
[4] Tel.: +81 75 751 3760; fax: +81 75 771 9709.

0720-048X/$ – see front matter © 2009 Elsevier Ireland Ltd. All rights reserved.
doi:10.1016/j.ejrad.2009.11.019

Please cite this article in press as: Nakatani K, et al. The potential clinical value of FDG-PET for recurrent renal cell carcinoma. Eur J Radiol (2009), doi:10.1016/j.ejrad.2009.11.019

2. Patients and methods

2.1. Patients

Between August 2000 and January 2008, 39 patients underwent 45 FDG-PET scans at our institute in order to investigate RCC. Among them, 8 patients (undergoing 8 scans) did not histologically prove to have RCC because they did not undergo surgery or biopsy, 1 patient (undergoing 1 scan) had bilateral renal tumors, one of which was not histologically proven, and 6 patients (undergoing 7 scans) had synchronous double cancer. These patients were excluded in our study. In this retrospective study, we reviewed records of 24 patients (18 men, 6 women; age range: 45–78 years, mean age: 63 years) who had histopathologically proven RCC and did not have synchronous malignant tumors. They underwent 29 PET scans. Periods from prior nephrectomy to PET scan ranged from 1 month to 27 years (average: 7.6 years, median: 3.5 years). All cases underwent both PET and CT scans and had prior CT scans. Each scan was performed within 6 months (18 scans within a month). All these studies involved daily clinical diagnostic checkups and written informed consent, requested by our institutional review board, was obtained from each patient.

2.2. PET scanning

Fluorine-18 FDG was synthesized by nucleophilic substitution method using an FDG synthesizing instrument (F-100, Sumitomo Heavy Industries, Tokyo, Japan) and a cyclotron (CYPRIS-325R, Sumitomo Heavy Industries, Tokyo, Japan). For 22 patients (27 scans) in this study, PET was performed using an Advance scanner (GE Healthcare, Milwaukee, WI, USA). For the remaining 2 patients (2 scans), PET was performed using a C-PET plus scanner (ADAC, Philadelphia, PA, USA). After fasting for at least 4 h, patients received intravenous administration of approximately 370 MBq (for the Advance scanner) or 130 MBq (for the C-PET plus scanner) of FDG, and whole-body PET images were acquired approximately 60 min later. Using the Advance scanner, each emission scan was obtained for 3 min per single bed position and each post-emission transmission scan was obtained for 1 min per single bed position. In order to cover from the skull base to the upper thigh, 5–6 bed positions were scanned according to the height of each patient. Images were acquired in 2-dimensional mode. The ordered subset expectation maximization algorithm using 16 subsets, 3 iterations, and a 128×128 matrix size reconstructed attenuation-corrected transaxial images. Data acquisition by the C-PET plus scanner was performed in 3-dimensional imaging mode with septae in place. Following a 56-s transmission scan, a whole body static image was then acquired for 6 min per bed position. The data were reconstructed using row action maximum likelihood algorithm.

2.3. CT scanning

CT scans were performed prior to PET scans using single or multidetector-row CT scanners (Aquillion 8, 16, or 64, Toshiba, Tokyo, Japan; W3000, Hitachi Medico, Tokyo, Japan; HiSpeed Advantage, GE Healthcare, Milwaukee, WI, USA). Thoracic and abdominal images were obtained separately or continuously with (19 scans) or without (10 scans) intravenous contrast material.

Table 1
Characteristics, results of images, and clinical outcomes of patients with RCC.

Pt. #	Age/Sex	Histology of prior specimen[a]			Result		Sites of metastases		Outcome
		Type	Grade	TNM	CT	PET	P/o by PET	Final Dx	
1	57/M	CCC	NA	NA	TP	TP	Lu	<u>*Lu*</u>	Rec.
	58/M				TN	FP	(Lu)[c]	None	Rec.
	60/M				TN	TN	None	None	Rec.
	61/M				FN	TP	LN	<u>*LN*</u>	No rec.
	62/M				TN	TN	None	None	No rec.
2	69/M	CCC	1	T3b	TN	TN	None	None	No rec.
3	54/M	CCC	2	T2a	FP	FP	(LN)[c]	None	No rec.
4	65/M	CCC	1	T2b	FP	TN	None	None	No rec.
5	76/M	CCC	2	T1a	TP	TP	Bo	Bo	Drop out (rec.)
	77/M				TP	TP	Bo	Bo, Lu	Drop out (rec.)
6	46/M	CCC	3	Tx	TP	TP	Ki, LN, Pe	Ki, LN, *Pe*	Death
7	52/M	CCC[b]	3	M1	TP	FN	None	Br, Lu	Rec.
8	77/M	CCC	2	T2	TP	TP	Bo, LN, Lu, Mu	Bo, Lu, LN, Mu, *Sk*	Death
9	62/M	CCC[b]	3	M1	TP	TP	Lu, Ad	Ad, Br, Lu	Death
10	58/M	PRC	2	T1a	TP	TP	Pe	Pe	Death
11	71/F	CCC[b]	3	T3b	TP	TP	Ad, Lo, Mu	Ad, Lo, *Mu*	Death
12	59/M	CCC	NA	NA	TP	TP	Pa	<u>*Pa*</u>	No rec.
13	58/M	CCC[b]	3	T1b	TP	FN	None	Ki, Pa, Thy	Rec.
14	73/F	CCC	NA	NA	TP	TP	Pa	<u>*Pa*</u>	No rec.
15	65/M	CCC	1	T2b	TP	TP	Pa	<u>*Pa*</u>	Drop out (rec.)
16	56/M	CCC	NA	T2	TP	FN	None	<u>*Pa*</u>	No rec.
17	66/M	PRC	3	M1	FN	TP	Bo	Bo	Death
18	54/F	PRC	3	M1	TP	TP	Ad, Bo, Lu	Ad, Bo, Lu	Death
19	78/M	NA	3	T1a	TP	TP	Lu	Lu	No rec.
20	45/F	PRC	2	T3b	TP	TP	Bo, LN, Lo, Mu	Bo, LN, Lo, *Mu*	Death
21	56/F	CCC	NA	NA	TP	FN	None	<u>*Li*</u>	Death
22	75/F	CCC	2	T1b	TN	TN	None	None	Death from pneumonia
23	64/M	CCC	3	M1	TP	TP	Bo, Li	Bo, *Li*	Drop out (rec.)

Abbreviations: Pt. #, patient number; F, female; M, male; CCC, clear cell carcinoma; PRC, papillary renal cell carcinoma; NA, not available; TP, true positive; TN, true negative; FP, false positive; FN, false negative; P/o, pointed out; Dx, diagnosis; Ad, adrenal gland; Bo, bone; Br, brain; Ki, contralateral kidney; Li, liver; LN, lymph node; Lo, local recurrence; Lu, lung; Mu, muscle; Pa, pancreas; Pe, peritoneal dissemination; Sk, skin; Thy, thyroid; Rec., recurrence.
Sites of metastases written in *oblique type* were biopsy-proven, and sites of metastases written in *oblique type and underlined* were surgically proven.
[a] Histological findings are based on the 3rd edition of the General Rule for Clinical and Pathological Studies on Renal Cell Carcinoma (in Japanese).
[b] With sarcomatoid component.
[c] False-positive lesion.

Please cite this article in press as: Nakatani K, et al. The potential clinical value of FDG-PET for recurrent renal cell carcinoma. Eur J Radiol (2009), doi:10.1016/j.ejrad.2009.11.019

2.4. Image interpretation and analysis

Interpretations of PET images were performed by consensus of at least two nuclear medicine physicians, with all available clinical information, including anatomical information provided by prior CT and/or other conventional imaging modalities. In this study, interpretation criteria were as follows; lesions were regarded as being an abnormal finding or representative of tumor if metabolic activity of FDG was moderately or markedly increased, relative to comparable normal structures or surrounding soft tissues. Findings provided by CT images, such as lesion size, shape, or enhancement patterns, were not taken into account for the purpose of the study. For example, a lesion with no or faint uptake of FDG was regarded as negative even if a recurrent tumor had been suspected by CT. Based on these criteria, the diagnostic accuracy of PET was estimated. Final diagnoses were made histopathologically or according to clinical follow-up using CT scans for at least 6 months.

When PET detected lesions that had not been observed by conventional imaging modalities, or when PET revealed characteristics of lesions other modalities interpreted inconclusively, the obtained finding was regarded as '*additional information*'. If patient treatments changed as a result of PET findings, these findings were considered to have offered '*clinical impact*'.

Patients were categorized into a PET-positive and a PET-negative group. Kaplan–Meier survival estimates were calculated from the first day of the PET scan to death.

3. Results

We evaluated a total of 28 PET scans in 23 patients and excluded 1 patient (using the Advance scanner) without definite final diagnosis. The patients' profile and their clinical outcome are shown in Table 1. Of 28 cases, 21 were finally confirmed to be in recurrence via surgery ($n = 7$), biopsy ($n = 8$), and clinical follow-up ($n = 6$), i.e. the tumor had increased in size. The remaining 7 cases were considered negative for recurrence. Histopathology demonstrated that the type of recurrent cases were clear cell RCC in 16 patients, papillary RCC in 4 patients, and unknown in 1 case.

The PET results were true-positives in 17 cases (clear cell RCC in 12 cases, papillary RCC in 4 cases, and unknown histology in 1 case). Fig. 1 demonstrates a true-positive case which gave additional information and clinical impact. On the other hand, PET failed to show recurrent lesions in 4 cases, all of which were clear cell RCC. These missed observations included 1 case of brain and lung metastases, 1 case of multiple small liver metastases, and 2 cases of metastases to the pancreas. Fig. 2 demonstrates 1 representative false-negative case. PET findings yielded false positive in 2 cases. One case revealed inflammatory changes in the lung and the other, mediastinal lymphadenitis. In the remaining 5 cases, the results of PET scans were true negative. As shown in Table 2, overall sensitivity, specificity, accuracy, positive predictive value, and negative predictive value were 81%, 71%, 79%, 90%, and 56%, respectively. When objects were confined to the cases with clinically suspected recurrence by prior CT images or by clinical symptoms, such as general malaise or long-lasting fever, the sensitivity, specificity,

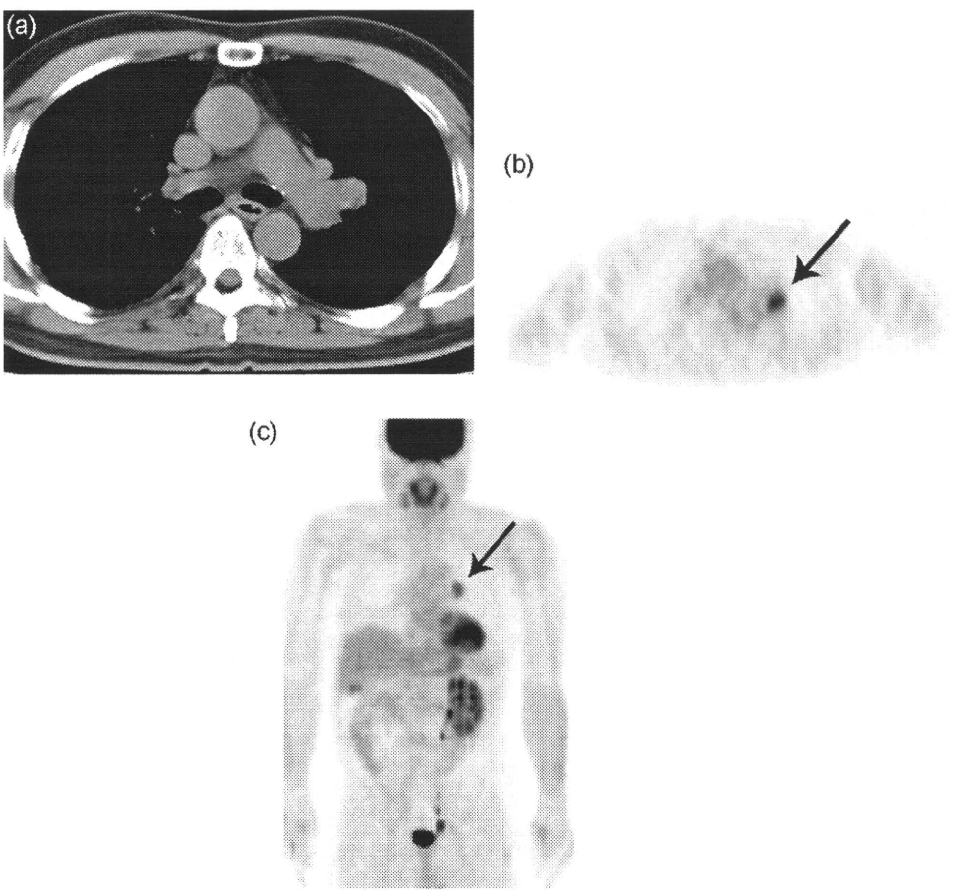

Fig. 1. A case of true-positive FDG-PET for metastatic renal cell carcinoma with additional information and clinical impact. An axial slice of unenhanced CT (a) and an axial slice (b) and maximum intensity projection (MIP) image (c) of FDG-PET are shown. A 61-year-old male (Pt. #1) respectively had a history of right nephrectomy and pulmonary metastasectomy 16 and 3 years earlier. He underwent unenhanced CT and no more lesions were found. PET showed significant uptake on the left hilar lymph node (arrows), indicating metastasis to the lymph node. Surgical resection was performed, and the lesion turned out to be a positive node.

Please cite this article in press as: Nakatani K, et al. The potential clinical value of FDG-PET for recurrent renal cell carcinoma. Eur J Radiol (2009), doi:10.1016/j.ejrad.2009.11.019

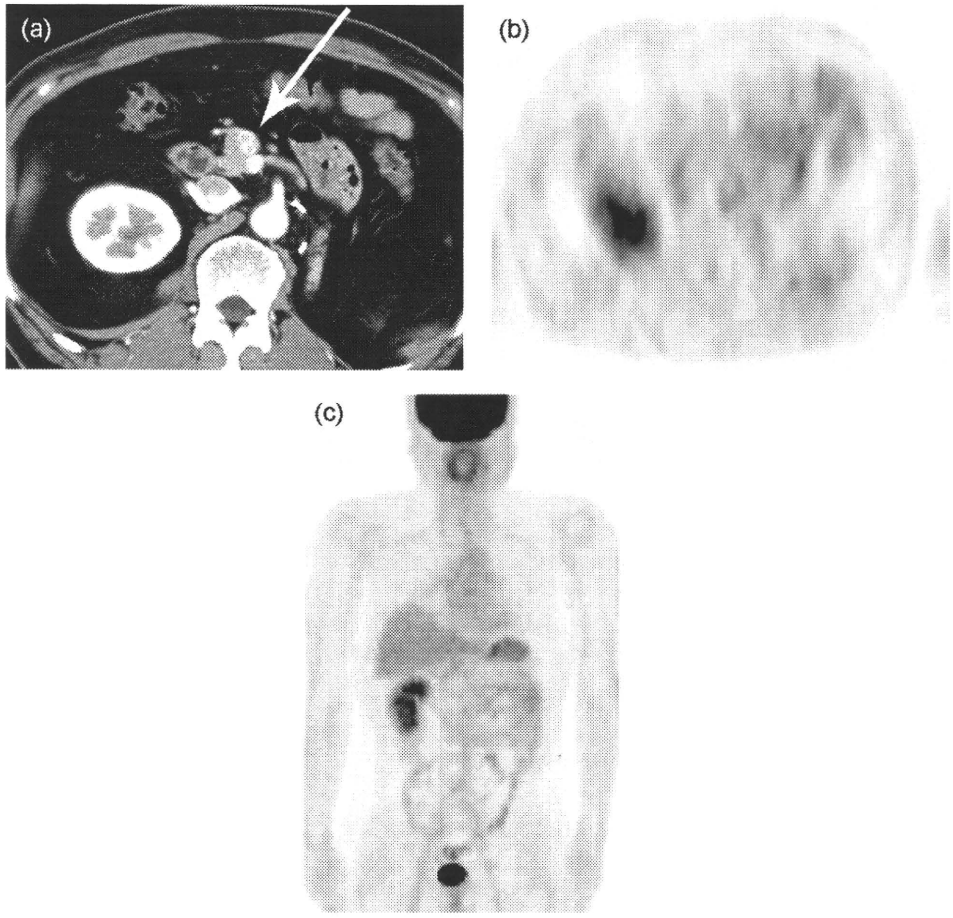

Fig. 2. A case of false-negative FDG-PET for metastatic renal cell carcinoma. An axial slice of arterial phase of enhanced CT (a) and an axial slice (b) and maximum intensity projection image (c) of FDG-PET are shown. A 56-year-old male (Pt. #16) underwent CT and was suspected of having metastasis. FDG-PET showed no significant uptake. The tumor was resected, and metastasis to the pancreas was histologically confirmed.

Table 2a
Cross-tabulation of the results of case-based analysis ($n = 28$).

		Final diagnosis	
		Recurrence (+)	Recurrence (−)
PET	Positive	17	2
	Negative	4	5

Sensitivity 81%, specificity 71%, accuracy 79%.

accuracy, positive predictive value, and negative predictive value of PET were 80%, 67%, 78%, 94%, and 33%, respectively.

All 4 false-negative cases had clear cell RCC, and the PET results in all 4 cases with papillary RCC were true-positive. However, there was no statistically significant difference about the diagnostic accuracy between the two histological subtypes according to Fisher's exact test ($p = 0.5376$). No correlation was found between nuclear grades of primary tumors and FDG uptake of recurrent tumors, either.

Table 2b
Cross-tabulation of the results of cases with suspected recurrence ($n = 23$).

		Final diagnosis	
		Recurrence (+)	Recurrence (−)
PET	Positive	16	1
	Negative	4	2

Sensitivity 80%, specificity 67%, accuracy 78%.

PET correctly detected local recurrence, peritoneal dissemination, bone metastases, muscle metastases, and adrenal metastases in all cases. On the other hand, sensitivities of metastases to the brain, thyroid, liver, or contralateral kidney were low, although the number of metastatic lesions was limited (Table 3). Fig. 3 demonstrates a case with metastases to the peritoneum and kidney.

'Additional information' over CT was obtained in 6 cases (21%). In 1 patient (No. 1), who had been thought to be disease-free by prior unenhanced CT, PET revealed a hilar lymph node metastasis which was confirmed histologically. In another patient (No. 17), whose prior CT image investigating the cause of general malaise

Table 3
Number of cases according to metastatic foci.

Metastatic organ	No. of total cases	No. of PET true-positive cases
Lung	7	5 (71.4%)
Mediastinal lymph node	3	2 (66.6%)
Abdominal lymph node	2	2 (100%)
Bone	7	7 (100%)
Contralateral kidney	2	1 (50%)
Brain	2	0 (0%)
Pancreas	5	3 (60%)
Adrenal gland	3	3 (100%)
Peritoneal dissemination	2	2 (100%)
Muscle	3	3 (100%)
Local recurrence	2	2 (100%)
Skin	1	0 (0%)
Liver	2	1 (50%)
Thyroid	1	0 (0%)

Please cite this article in press as: Nakatani K, et al. The potential clinical value of FDG-PET for recurrent renal cell carcinoma. Eur J Radiol (2009), doi:10.1016/j.ejrad.2009.11.019

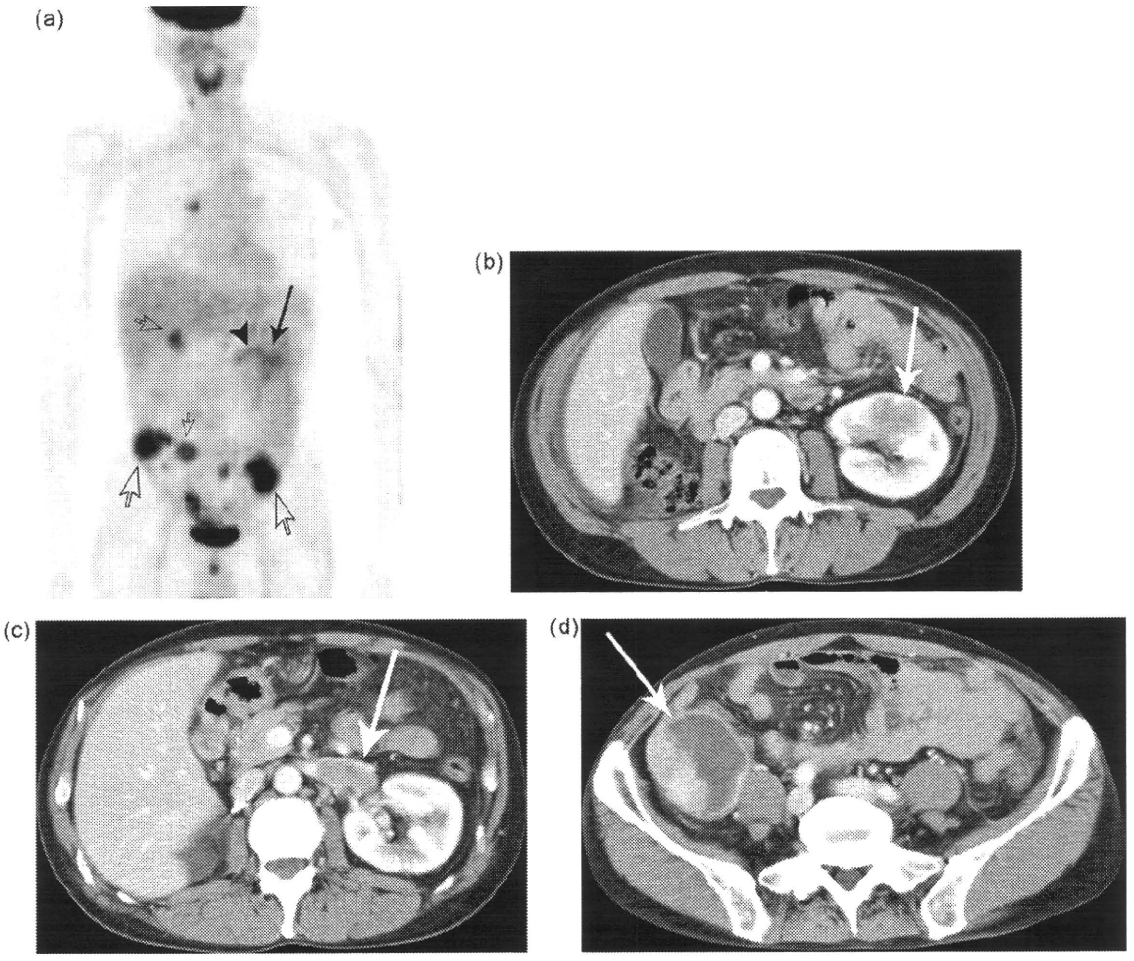

Fig. 3. A case with metastatic renal cell carcinoma to the peritoneum, right hilar nodes, and left kidney. A maximum intensity projection image of FDG-PET (a) and axial slices of enhanced CT (b–d) are demonstrated. Metastatic lesions to the contralateral kidney (a: black arrow, b: white arrow) and to the peritoneum (a, d: white arrows) were identified as FDG-avid foci. Tumor thrombus in the left renal vein is also seen on PET and CT (a: arrowhead, c: white arrow).

has not shown any remarkable findings, PET showed diffuse bone marrow metastases that were later biopsy-proven. In patient No. 20, PET discovered an unknown chest wall metastasis on her back, for which excision and irradiation therapy was performed. For these 3 patients, the PET findings were considered to yield 'clinical impacts'. In the remaining 3 patients, PET additionally revealed an adrenal gland metastasis, a sternal bone metastasis, and vertebral metastases, but their clinical management did not change.

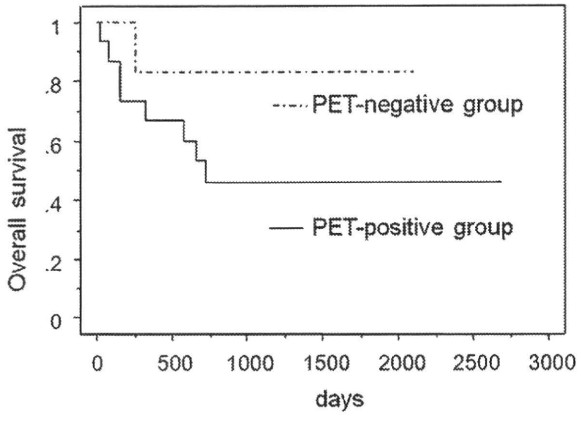

Fig. 4. The overall survival of the PET-positive group including 16 patients (solid line) and the PET-negative group including 6 patients (dashed line). The PET-positive group tended to have a poorer prognosis, but was not statistically significantly different ($p = 0.1739$).

Among the 23 patients for whom final diagnoses were obtained, 1 female patient died of pneumonia irrelevant to cancer. The survival analysis was, therefore, performed after excluding this patient. During their follow-up periods, ranging from 6 to 2691 days with the median of 711 days, 9 patients died of primary disease. Of these patients, 8 belonged to the PET-positive group (16 patients) and 1 patient, who died of liver failure due to multiple liver metastases, belonged to the PET-negative group (6 patients). Cumulative survival rates over 5 years in the PET-positive group and in the PET-negative group were 46% and 83%, respectively, as presented by Kaplan–Meier survival curves (Fig. 4). The difference between the two groups did not reach statistical significance according to the log-rank test ($\chi^2 = 1.849$, $p = 0.1739$).

4. Discussion

The overall diagnostic performance of FDG-PET for recurrent RCC after nephrectomy was reasonably high, with a case-based sensitivity of 81%, specificity of 71%, and accuracy of 79%, which was considered comparable with those for other malignancies. These data indicate that FDG-PET would be a useful tool for postoperative surveillance even in patients with RCC.

Please cite this article in press as: Nakatani K, et al. The potential clinical value of FDG-PET for recurrent renal cell carcinoma. Eur J Radiol (2009), doi:10.1016/j.ejrad.2009.11.019

The role of FDG-PET for re-staging of RCC was initially examined by Safaei et al., who examined 36 patients and demonstrated the sensitivity, specificity, and accuracy of 87%, 100%, and 89%, respectively [8]. According to published reports, overall sensitivity and specificity of FDG-PET for re-staging were 64–87% and 75–100% [8–10]. Our data were almost consistent with these observations. As for initial diagnosis and staging of primary RCC, overall sensitivity of FDG-PET varied, ranging from 32% to 100% [1–7]. The largest study by Kang et al. showed a sensitivity of 60% [7], raising questions as to the clinical value of FDG-PET. FDG-PET may be helpful in the evaluation of recurrent RCC rather than in initial staging of RCC.

In general, there are many RCC that are not FDG-avid, with the reason behind this phenomenon remaining unclear. For example, Miyauchi et al. reported that renal cancers in their series of 11 patients with newly diagnosed RCC were well visualized with FDG-PET, had higher grade, higher glucose transporter-1 (GLUT-1) expression and tended to be larger than poorly imaged cancers (Miyauchi T et al., presented at the 1996 annual meeting of the Society of Nuclear Medicine).

In contrast, Miyakita et al. stated that there was no correlation between GLUT-1 expression and FDG-PET positivity [5]. Montravers et al. formulated the hypothesis that mild or absent FDG contrast observed in primary RCC was due to a lack of accessibility of radiotracers to tumor cells [3,16].

As compared with primary tumors, it seems that recurrent or metastatic foci of RCC tended to be FDG-avid, resulting in higher sensitivity of FDG-PET, although a few recurrent tumors were not FDG-avid. In our study, uptake of FDG in recurrent tumors was not statistically correlated with histological type, nuclear grade, or presence of sarcomatoid components, as it is demonstrated in Table 1. This might be because of the small number of cases. Further examination with increased number of cases with various histological types might be needed. One of the reasons explaining the difference in the diagnostic performance could be attributed to the urinary system. FDG is excreted into urine yielding substantial tracer accumulation in a renal collecting system, and thus accumulation in primary RCC is sometimes obscured by or misrecognized as excretion itself [2,8,17]. FDG accumulation in metastatic tumors is not obscured by excretion, except in the contralateral kidney. Physiological uptake of FDG in background tissue can mask accumulation into tumors in liver, brain, and kidney. In fact, tumors metastasized to these organs tended to be missed in our population, although the number of the lesions was limited. Nevertheless, as shown in Fig. 3, there was a case in which a metastasis to kidney was identified because of FDG uptake in the tumor thrombus directly invading to a renal vein that could be easily distinguished from urinary tract.

Understanding how often additional information is obtained if FDG-PET is used in conjunction with morphological information, usually acquired by CT, is important in assessing the clinical utility of this technique. In our study, 'additional information' over CT was obtained in 6 cases (21%), causing an alteration of therapeutic plans in 3 of these cases (11%). Among these cases, 2 patients (7%) who had been regarded as disease-free by prior CT turned out to have recurrence that was detected using PET. However, several reports noted that metastasectomy under the appropriate conditions can bring survival benefits in selected patients [11–15]. A tumor-free interval of more than 2 years between primary tumor and metastasis was reported to be accompanied by a longer disease-specific survival after successful metastasectomy [11]. Moreover, molecular-targeted therapies with multi-kinase inhibitors such as sorafenib and sunitinib are now recommended as preferential therapy against metastatic RCC. Therefore, it is essential for starting these strategies to point out correct metastatic sites. In addition, there are no reliable specific tumor markers for RCC, although erythrocyte sedimentation rate (ESR), C-reactive protein (CRP), and serum immunosuppressive acidic protein (IAP) have been proposed to be a prognostic factor [18–20]. Therefore, the diagnostic imaging for evaluation of recurrence, including FDG-PET, may be helpful, even if clinical impacts cannot be obtained very frequently. Indeed, although postoperative surveillance is generally performed using CT, patients with renal insufficiency after nephrectomy are not permitted to perform CT with IV contrast material. CT without IV contrast provides limited information in pointing out unexpected metastases. Since renal carcinomas have a tendency to metastasize to a variety of organs, it would be difficult to detect metastases to pancreas or muscle only by unenhanced CT. Especially in these cases, we believe that FDG-PET (or PET/CT) can be effectively applicable.

In survival time analysis, the PET-positive group tended to have poorer prognosis, but the difference of cumulative survival rates between the two groups did not reach statistical significance. One of the reasons might be the small number of cases. We need to perform a further investigation using an increased number of cases to conclude prognostic value of FDG-PET for recurrent RCC. In addition, the kind of adjuvant therapy the patients received, or whether metastatic tumors were successfully removed after being found, was not taken into account in the present analysis. Survival curves for both the PET-positive and PET-negative group were ultimately plateau. This observation may have been affected as a result of the removal of metastatic tumors, already being advocated as one independent prognostic factor [11–15].

The present study had several limitations. This study was not prospective, and the study population may have a bias. Clinical follow-up after nephrectomy was usually performed using a CT scan, whereas FDG-PET was performed only in limited cases. Indeed, in the present study, patients whose prior CT scan suggested presence of recurrent tumors were the vast majority, and so the overall prevalence of recurrence in the study was as high as 75%. If clinical follow-up after nephrectomy had been performed using FDG-PET first, the prevalence of recurrence would not have been so high and the diagnostic accuracy might have been different. The prior CT scans were not standardized either as enhanced CT or as unenhanced CT. FDG-PET/CT is often reported superior to FDG-PET alone. In spite of these limitations, we believe that our study could favor the use of FDG-PET for postoperative surveillance in patients with RCC, and throughout almost 10 years of our institution's experience, we could undertake to determine whether FDG uptake could be a predictor of survival.

In conclusion, FDG-PET can be a complementary modality for postoperative surveillance in patients with RCC. Further investigations are needed to conclude whether PET can yield a prognostic value.

References

[1] Wahl RL, Harney J, Hutchins G, Grossman HB. Imaging of renal cancer using positron emission tomography with 2-deoxy-2-(18F)-fluoro-D-glucose: pilot animal and human studies. J Urol 1991;146(6):1470–4.
[2] Goldberg MA, Mayo-Smith WW, Papanicolaou N, Fischman AJ, Lee MJ. FDG PET characterization of renal masses: preliminary experience. Clin Radiol 1997;52(7):510–5.
[3] Montravers F, Grahek D, Kerrou K, et al. Evaluation of FDG uptake by renal malignancies (primary tumor or metastases) using a coincidence detection gamma camera. J Nucl Med 2000;41(1):78–84.
[4] Ramdave S, Thomas GW, Berlangieri SU, et al. Clinical role of F-18 fluorodeoxyglucose positron emission tomography for detection and management of renal cell carcinoma. J Urol 2001;166(3):825–30.
[5] Miyakita H, Tokunaga M, Onda H, et al. Significance of 18F-fluorodeoxyglucose positron emission tomography (FDG-PET) for detection of renal cell carcinoma and immunohistochemical glucose transporter 1 (GLUT-1) expression in the cancer. Int J Urol 2002;9(1):15–8.
[6] Aide N, Cappele O, Bottet P, et al. Efficiency of [(18)F]FDG PET in characterising renal cancer and detecting distant metastases: a comparison with CT. Eur J Nucl Med Mol Imaging 2003;30(9):1236–45.

Please cite this article in press as: Nakatani K, et al. The potential clinical value of FDG-PET for recurrent renal cell carcinoma. Eur J Radiol (2009), doi:10.1016/j.ejrad.2009.11.019

[7] Kang DE, White Jr RL, Zuger JH, Sasser HC, Teigland CM. Clinical use of fluorodeoxyglucose F 18 positron emission tomography for detection of renal cell carcinoma. J Urol 2004;171(5):1806–9.
[8] Safaei A, Figlin R, Hoh CK, et al. The usefulness of F-18 deoxyglucose whole-body positron emission tomography (PET) for re-staging of renal cell cancer. Clin Nephrol 2002;57(1):56–62.
[9] Majhail NS, Urbain JL, Albani JM, et al. F-18 fluorodeoxyglucose positron emission tomography in the evaluation of distant metastases from renal cell carcinoma. J Clin Oncol 2003;21(21):3995–4000.
[10] Jadvar H, Kherbache HM, Pinski JK, Conti PS. Diagnostic role of [F-18]-FDG positron emission tomography in restaging renal cell carcinoma. Clin Nephrol 2003;60(6):395–400.
[11] van der Poel HG, Roukema JA, Horenblas S, van Geel AN, Debruyne FM. Metastasectomy in renal cell carcinoma: a multicenter retrospective analysis. Eur Urol 1999;35(3):197–203.
[12] Antonelli A, Zani D, Cozzoli A, Cunico SC. Surgical treatment of metastases from renal cell carcinoma. Arch Ital Urol Androl 2005;77(2):125–8.
[13] Leibovich BC, Cheville JC, Lohse CM, et al. A scoring algorithm to predict survival for patients with metastatic clear cell renal cell carcinoma: a stratification tool for prospective clinical trials. J Urol 2005;174(5):1759–63.
[14] Eggener SE, Yossepowitch O, Kundu S, Motzer RJ, Russo P. Risk score and metastasectomy independently impact prognosis of patients with recurrent renal cell carcinoma. J Urol 2008;180(3):873–8.
[15] Crispen PL, Boorjian SA, Lohse CM, Leibovich BC, Kwon ED. Predicting disease progression after nephrectomy for localized renal cell carcinoma: the utility of prognostic models and molecular biomarkers. Cancer 2008;113(3):450–60.
[16] Montravers F, Rousseau C, Doublet JD, et al. In vivo inaccessibility of somatostatin receptors to 111In-pentreotide in primary renal cell carcinoma. Nucl Med Commun 1998;19(10):953–61.
[17] Gallagher BM, Fowler JS, Gutterson NI, MacGregor RR, Wan CN, Wolf AP. Metabolic trapping as a principle of radiopharmaceutical design: some factors responsible for the biodistribution of [18F] 2-deoxy-2-fluoro-D-glucose. J Nucl Med 1978;19(10):1154–61.
[18] Sengupta S, Lohse CM, Cheville JC, et al. The preoperative erythrocyte sedimentation rate is an independent prognostic factor in renal cell carcinoma. Cancer 2006;106(2):304–12.
[19] Lamb GW, McMillan DC, Ramsey S, Aitchison M. The relationship between the preoperative systemic inflammatory response and cancer-specific survival in patients undergoing potentially curative resection for renal clear cell cancer. Br J Cancer 2006;94(6):781–4.
[20] Araki K, Igarashi T, Tobe T, et al. Serum immunosuppressive acidic protein doubling time as a prognostic factor for recurrent renal cell carcinoma after nephrectomy. Urology 2006;68(6):1178–82.

Please cite this article in press as: Nakatani K, et al. The potential clinical value of FDG-PET for recurrent renal cell carcinoma. Eur J Radiol (2009), doi:10.1016/j.ejrad.2009.11.019

Eur J Nucl Med Mol Imaging (2010) 37:468–482
DOI 10.1007/s00259-009-1284-9

ORIGINAL ARTICLE

FDG PET as a prognostic predictor in the early post-therapeutic evaluation for unresectable hepatocellular carcinoma

Tatsuya Higashi · Etsuro Hatano · Iwao Ikai · Ryuichi Nishii · Yuji Nakamoto · Koichi Ishizu · Tsuyoshi Suga · Hidekazu Kawashima · Kaori Togashi · Satoru Seo · Koji Kitamura · Yasuji Takada · Shinji Kamimoto

Received: 11 June 2009 / Accepted: 4 September 2009 / Published online: 17 October 2009

Abstract
Purpose To elucidate the prognostic role of post-therapeutic ^{18}F-fluorodeoxyglucose (^{18}F-FDG) positron emission tomography (PET), we conducted a retrospective cohort study analysing the clinical factors that affect overall survival after non-operative therapy for unresectable hepatocellular carcinoma (HCC).
Methods Sixty-seven cases with unresectable HCC who received non-operative therapy (transcatheter arterial chemoembolization: n=24, transcatheter arterial infusion chemotherapy: n=31, radiofrequency ablation: n=5 or systemic chemotherapy: n=7) and had received FDG PET for the evaluation of the therapeutic effect within 1 month after the end of the therapy were evaluated. Overall survival rate was evaluated using the univariate and multivariate analyses of relevant clinical and laboratory parameters before and after therapy, including visual PET analysis and quantitative analysis using maximum standardized uptake value (SUV).
Results Visual PET diagnosis of post-therapeutic lesions was a good predictor of overall survival of unresectable HCC patients. The low FDG group showed significantly longer survival (average: 608 days) than that (average: 328 days) of the high FDG group (p<0.0001). Multivariate analysis showed four significant prognostic factors for the survival: post-therapeutic alpha-fetoprotein (αFP) level (=400 ng/ml, p=0.004), post-therapeutic visual PET diagnosis (p=0.006), post-therapeutic clinical stage (UICC stage IV, p=0.04) and post-therapeutic Milan criteria (p=0.03), while pre-therapeutic clinical factors, SUV by post-therapeutic FDG PET (5.0 or more) or others did not show significance.
Conclusion The present study suggests that post-therapeutic PET performed within 1 month after non-operative therapy can be a good predictor of overall survival in unresectable HCC patients, while pre-therapeutic evaluation including PET, tumour markers and clinical staging may not be useful.

Keyword FDG · Hepatocellular carcinoma · PET · Early prediction · Prognosis · Response · Non-operative therapy

T. Higashi (✉) · R. Nishii
Shiga Medical Center Research Institute,
5-4-30, Moriyama,
Moriyama City, Shiga 524-8524, Japan
e-mail: higashi@shigamed.jp

E. Hatano · I. Ikai · S. Seo · K. Kitamura · Y. Takada · S. Kamimoto
Department of Gastroenterological Surgery,
Kyoto University Graduate School of Medicine,
54 Kawahara-cho, Shogoin,
Sakyo-ku, Kyoto 606-8507, Japan

Y. Nakamoto · K. Ishizu · T. Suga · H. Kawashima · K. Togashi
Department of Diagnostic Imaging and Nuclear Medicine,
Kyoto University Graduate School of Medicine,
54 Kawahara-cho, Shogoin,
Sakyo-ku, Kyoto 606-8507, Japan

Introduction

Hepatocellular carcinoma (HCC) is one of the most frequently occurring tumours worldwide and ranks fifth in frequency in the world [1, 2]. Resection and transplantation achieve the best outcomes in well-selected candidates; however, the 5-year survival rate is only 60–70% [3, 4].

Therefore, a large proportion of patients with HCC were treated with non-operative therapy, because of high risk factors, such as non-localized multiple intrahepatic lesions, extensive vascular invasion or extrahepatic metastasis or because of the shortage of donor livers for transplantation. At the present time, transcatheter arterial chemoembolization (TACE) and transcatheter arterial infusion chemotherapy (TAI) are the main non-operative therapies for relatively large or advanced intrahepatic HCC, while radiofrequency ablation (RFA) and percutaneous ethanol injection therapy (PEIT) are the main non-operative therapies for relatively small HCCs which present in small quantities [5]. For patients with distant metastasis, systemic chemotherapy is supposed to be the best choice. Recently, sorafenib, a multi-targeted tyrosine kinase inhibitor, was found to improve survival of patients with advanced stage HCC [6]. The clinical role of non-operative therapies will become more important in the near future.

In general, the therapeutic response of HCC to non-operative therapy is assessed by conventional radiological imaging modalities, based on the Response Evaluation Criteria in Solid Tumors [7]. However, such criteria using conventional imaging modalities have shown their limitations because therapeutic response and tumour viability are not appropriately reflected in patients with HCC [8]. It was reported in post-operative HCC patients that intrahepatic recurrence could be predicted by several factors, such as the presence of microvascular invasion, poor histological differentiation and satellite lesions [9, 10]. However, these factors based on pathological evaluation cannot be utilized for the evaluation of patients with unresectable HCC treated with non-operative therapy. There is really a call for an appropriate indicator of tumour viability and a predictor of prognosis in patients after non-operative therapy, especially one using a non-invasive imaging modality.

The uptake of ^{18}F fluorodeoxyglucose (^{18}F-FDG), based on the enhanced glucose metabolism in cancer cells, is supposed to be a sensitive marker of tumour viability. Tumour detection using increased ^{18}F-FDG uptake by positron emission tomography (PET) has therefore been applied in diagnostic imaging for a variety of tumours, including HCC [11, 12]. Several studies in liver tumours have shown that FDG PET is useful for tumour characterization, assessment of therapeutic response and outcome [13–15]. On the other hand, other reports showed that the sensitivity of FDG PET is not sufficiently high (50–55%) in HCC patients [16–19]. Recently, concerning resectable HCC, our group reported that FDG uptake evaluated by pre-operative PET is associated with tumour differentiation and post-operative survival in HCC patients treated with partial hepatectomy [20, 21]. However, there has been no report regarding the relationship between prognosis and FDG uptake evaluated by post-therapeutic PET after non-operative therapy in patients with unresectable HCC.

The purpose of this study is to investigate retrospectively the efficacy of FDG PET as an in vivo marker for tumour viability of HCC after non-operative therapy and as a prognostic predictor for post-treatment overall survival in patients with unresectable HCC.

Materials and methods

Study population

From May 2003 to April 2008, 465 cases with HCC were admitted to our unit in Kyoto University Hospital for the wish to receive a radical operation or non-operative therapy. By computed tomography (CT) scan, magnetic resonance imaging (MRI) and other imaging modalities, 320 cases were diagnosed to be candidates for a curative operation and underwent surgery. Another 23 cases were diagnosed as having far-advanced HCC and only received palliative treatment. The other 122 cases were diagnosed as having unresectable HCC and treated by non-operative therapy. Inclusion criteria in the present study were as follows: (1) diagnosed as unresectable HCC by CT scan and MRI in pre-therapeutic evaluation, (2) treated with non-operative therapy (TACE, TAI, RFA, PEIT or systemic chemotherapy) and completed a single course of a therapeutic regimen, (3) diagnosed by FDG PET within 1 month after the end of non-operative therapy and (4) clinical follow-up more than 6 months after non-operative therapy. Exclusion criteria were as follows: (1) patients who received FDG PET only before non-operative therapy and (2) patients who received FDG PET more than 1 month after the end of non-operative therapy.

Of 122 cases with unresectable HCC, 67 were included in the present study, where 67 consecutive post-therapeutic FDG PET studies were performed in 58 patients within 1 month after the end of non-operative therapy (ranging from 0 to 28 days, mean interval of days: 10.9±10.9 days). In 29 patients, pre-therapeutic FDG PET was also performed within 3 months before the start of the therapy. Nine patients received non-operative therapies two times, with an interval of more than 1 month between each therapy (ranging from 32 to 1,960 days, mean interval of days: 328.5 days). Therefore, the patient who received non-operative therapies twice was counted as two cases for diagnosis of lesion viability and counted as a single patient at the time of the last post-therapeutic PET for analysis of survival. Finally, in this retrospective analysis, 67 cases (55 men and 12 women, mean age: 59.3±12.6 years) were analysed for diagnosis of lesion viability and 58 patients (46 men and 12 women, mean age: 60.8±12.1 years) were analysed for prediction of survival.

Before admission to Kyoto University Hospital, each patient gave written informed consent to becoming a possible candidate for retrospective clinical research (except for gene-

related researches), as required by the Kyoto University Human Study Committee.

Patient characteristics

Patient characteristics of 67 cases are shown in Table 1. The chemotherapeutic agents used in TACE, TAI and systemic chemotherapy were as follows: fluorouracil (5-FU) and 5-FU with cisplatin (CDDP) for TACE; 5-FU with CDDP and 5-FU with interferon for TAI; 5-FU, Farmorubicin (Farm) and gemcitabine (GEM) for systemic chemotherapy. The clinical stage of HCC was analysed at first before the treatment based on the criteria of the International Union Against Cancer (UICC) using several imaging modalities (CT, MRI and/or angiography and/or PET if available) [22]. The clinical stage of HCC was re-analysed at the time of post-therapeutic PET based on UICC criteria using PET results and other imaging modalities. Analyses using Milan criteria for the selection of liver transplantation were evaluated before the treatment based on the size and the number of tumours determined from imaging modalities using CT or MRI (single tumour: 5 cm or less in size; or three or less tumours: each 3 cm or less in size; and no macrovascular invasion) [23]. Analyses using Milan criteria were also re-evaluated at the time of post-therapeutic PET based on imaging modalities including PET. Thirty-seven patients

Table 1 Patient characteristics of 67 cases (58 patients)

Characteristic	Value	Characteristic	Value
Age (years)		Past history of therapy[a], *n* (%)	
Mean±SD	59.3±12.6	Partial resection	33 (49)
Range	32–80	LDLT	2 (3)
Gender, *n* (%)		TACE	51 (76)
Male	55 (82)	TAI	38 (57)
Female	12 (18)	RFA	31 (46)
Tumour differentiation, *n* (%)		PEIT	12 (18)
Well	3 (4)	Child-Pugh classification at pre-treatment, *n* (%)	
Moderately	16 (24)	A	38 (57)
Poorly	20 (30)	B	29 (43)
Unknown	28 (42)	Child-Pugh classification at PET study, *n* (%)	
Target therapy in the present study, *n* (%)		A	38 (57)
TACE	23 (34)	B	26 (39)
TAI	30 (45)	C	3 (4)
RFA	5 (7)	Child-Pugh score at PET study	
TACE+PEIT	1 (1)	Mean±SD	6.4±1.4
TAI+RFA	1 (1)	Aetiology of hepatitis, *n* (%)	
Systemic chemotherapy	7 (10)	HBV	19 (28)
Clinical stage at pre-treatment, *n* (%)		HCV	40 (60)
UICC, 6th edition		HBV+HCV	4 (6)
Stage II–III	47 (70)	Alcoholic	2 (3)
Stage IV	20 (30)	Unknown	2 (3)
Milan criteria at pre-treatment, *n* (%)		Pathological evaluation of hepatic parenchyma	
Fulfilled	21 (31)	Grade of hepatitis, *n* (%)	
Beyond	46 (69)	None	2 (3)
Clinical stage at post-PET evaluation, *n* (%)		Low	22 (38)
UICC, 6th edition		Moderate	12 (21)
Stage II–III	39 (58)	High	1 (2)
Stage IV	28 (42)	Not available	30 (36)
Milan criteria at post-PET evaluation, *n* (%)		Grade of fibrosis, *n* (%)	
Fulfilled	18 (27)	None	3 (5)
Beyond	49 (73)	Low	9 (16)
		Moderate	7 (12)
		High	18 (31)
		Not available	30 (36)

UICC International Union Against Cancer, TNM classification, *PET* positron emission tomography, *TACE* transcatheter arterial chemoembolization therapy, *TAI* transcatheter arterial infusion chemotherapy, *RFA* radiofrequency ablation therapy, *PEIT* percutaneous ethanol injection therapy, *LDLT* living donar liver transplantation, *HBV* hepatitis B virus, *HCV* hepatitis C virus

[a] Including overlapping therapy

received pathological evaluation of lesions and surrounding liver parenchyma by biopsy at the time of RFA or PEIT (at the present therapy or at the previous one within 6 months before the present therapy, $n=27$) or by surgical resection (within 2 weeks after the post-therapeutic PET, $n=10$). Activity grades of hepatitis and fibrosis were also evaluated in surrounding liver parenchyma by well-experienced pathologists using four-grade scales.

Tumour markers, including serum alpha-fetoprotein (αFP), lens culinaris agglutinin-reactive fraction of serum αFP (αFP-L3 fraction) and protein induced by vitamin K absence or antagonist II (PIVKA-II), were evaluated before the non-operative therapy and at the time of post-therapeutic PET. The presence of positive results in all these three tumour markers (αFP=400 or more, αFP-L3=15 or more and PIVKA-II=400 or more) was defined as "triple plus".

PET study

^{18}F was produced by ^{18}O(p, n) ^{18}F reaction. ^{18}F-FDG was synthesized by the nucleophilic substitution method using an ^{18}F-FDG-synthesizing instrument F-100 (Sumitomo Heavy Industries, Co. Ltd., Tokyo, Japan) and a cyclotron, CYPRIS-325R (Sumitomo Heavy Industries, Co. Ltd., Tokyo, Japan). All patients were examined with a whole-body PET scanner with an 18-ring detector arrangement (Advance, General Electric Medical Systems, Milwaukee, WI, USA).

The patients fasted for more than 4 h before the injection of ^{18}F-FDG. All subjects received an intravenous injection of ^{18}F-FDG (296 ±74 MBq), and the acquisition of whole-body PET images started 50 min later. Data acquisition (emission and transmission scan) was performed in two-dimensional imaging mode with septae in place. Emission images were acquired for 3 min per bed position and each post-emission transmission scan was obtained for 1 min per position. Whole-body scanning (from head to upper thigh) was performed in each patient using five or six bed positions according to the height of each patient. The data were reconstructed using the ordered subsets expectation maximization method (OSEM) using 16 subsets, 3 iterations and 128×128 array size.

Image analysis

PET images were interpreted and analysed visually by two or three experienced nuclear medicine physicians (TH, YN, KI, TS) with all available clinical information. Next, these physicians had a discussion and made a final diagnosis. Diagnosis of lesion viability was performed separately in liver lesions and metastatic lesions with a two-category system, positive or negative. In the diagnosis of liver lesions, FDG uptake of a lesion was compared with background uptake of liver parenchyma. If a nodule showed remarkably higher uptake than the liver parenchyma, PET diagnosis was defined as positive. If a nodule showed similar or lower uptake than the surrounding liver parenchyma, PET diagnosis was defined as negative. In the diagnosis of metastatic lesions, FDG uptake of each lesion was compared with background uptake of surrounding normal tissue or with the contralateral normal tissue (when the lesion was located in the lung field). All PET diagnostic results were based on the diagnostic reports described in patient charts at the time of the clinical course, and the whole results were again confirmed by nuclear medicine physicians (TH, RN) with 100% concordance rate, retrospectively. When visual PET analysis was negative in the whole body and then known lesions or newly discovered metastatic lesions were confirmed as alive within 6 months after PET study, visual PET diagnosis on lesion viability was defined as false-negative. On the contrary, when visual PET analysis was positive in a lesion and the lesion was confirmed as necrotic or nonexistent within 6 months after PET study, visual PET diagnosis on lesion viability was defined as false-positive. For univariate and multivariate analysis of prognostic factors, a positive PET finding in any lesion in the body (hepatic or metastatic, known or unexpected) was defined as positive for the patient.

In addition, semi-quantitative analysis of ^{18}F-FDG uptake was also performed for univariate and multivariate analysis of prognostic factors. Regions of interest (ROIs) were defined on the target lesions in the transaxial tomograms of PET images by the PET-to-CT co-registration method using the automatic rigid/non-rigid body-deformable fusion software: Quantiva/BodyGuide (Tomographix IP Ltd., Toronto, Canada). The maximum standardized uptake value (SUV) was calculated for quantitative analysis of tumour ^{18}F-FDG uptake as follows:

$$\mathrm{SUV} = \frac{\mathrm{C(kBq/ml)}}{\mathrm{ID(kBq)/body\ weight\ (g)}}$$

where C represents tissue activity concentration measured by PET and ID represents the injected dose. The highest maximum SUV of the lesion in the whole body (hepatic or metastatic) was defined as the SUV of the patient.

Clinical confirmation

Lesion viability after treatment was confirmed by surgical resection in ten cases (surgery could be performed later because of the therapeutic effect of non-operative therapy) and by clinical follow-up at least more than 6 months in 57 cases. Overall survival was confirmed in patient records by clinical follow-up at least more than 6 months, in which patients received at least one of several imaging modalities as follow-up study every 3 months, including CT, MRI, angiography

and PET. The starting point and the end-point of survival were defined as the date of post-therapeutic PET study and the date of death, respectively. Overall cumulative survival rates were obtained using the Kaplan-Meier method.

Statistics

All values are expressed as mean±SD. All of the statistical analysis was performed using statistical software, JMP 4 J version (SAS Institute, Cary, NC, USA), in which p values <0.05 were considered statistically significant. Patients were stratified and analysed by univariate analysis using the log-rank test according to the following factors: age, gender, histological grade of tumour differentiation, type of non-operative target therapy in the present study, clinical stage at pre-treatment evaluation (UICC), Milan criteria at pre-treatment evaluation, clinical stage at post-PET evaluation (UICC), Milan criteria at post-PET evaluation, past history of therapy, Child-Pugh classification, aetiology of hepatitis, pathological grade of hepatitis, pathological grade of fibrosis as well as pre-therapeutic and post-therapeutic tumour markers, including serum αFP level, serum αFP-L3 fraction, PIVKA-II level and triple plus, and pre-therapeutic and post-therapeutic FDG PET-related factors [SUV and visual PET diagnosis (positive or negative)]. Cut-off values, such as αFP=400 ng/ml, αFP-L3=15%, PIVKA-II=400 AU/ml and SUV=5.0, were defined based on the previous reports [21, 24, 25]. According to the univariate analysis, eight significant factors [clinical stage at post-PET evaluation (UICC), Milan criteria at post-PET evaluation, Child-Pugh classification, pathological grade of hepatitis, αFP level, presence of triple plus, SUV and visual PET diagnosis] were selected for the multivariate analysis using the stratified Cox proportional hazards model. A comparison between high FDG and low FDG groups was analysed by Wilcoxon score or chi-square test for unpaired data. Survival curves were calculated by Kaplan-Meier analysis and the differences between high FDG and low FDG groups and the differences between L-L, L-H, H-L and H-H groups were compared using the log-rank test.

Results

Patient characteristics

Table 1 summarizes the patient characteristics. The average follow-up of living patients (n=35) was 483±413 days (range: 202–1,565 days), while the average follow-up of dead patients (n=23) was 253±162 days (range: 22–644 days). The clinical stage at pre-treatment was evaluated as stage II–III (n=47, 70%) vs stage IV (n=20, 30%) by UICC. However, the clinical stage at post-PET was stage II–III (n=39, 58%) vs stage IV (n=28, 42%) by UICC. This is because an unexpected distant metastasis was detected by post-therapeutic PET study in 13% of patients (n=9) and PET refuted the presence of a distant metastasis in 1% of patients (n=1). Similar results were observed in Milan criteria.

Diagnosis of lesion viability

Table 2 shows the results of clinical values of post-therapeutic FDG PET as the diagnosis of lesion viability and as the survival prediction in unresectable HCC patients.

As for visual diagnosis of lesion viability of post-therapeutic hepatic lesions, sensitivity was relatively low with the value of 62.8% (27/43 cases), while positive predictive value was high with the value of 96.4% (27/28 cases). Sixteen false-negative PET cases (37.2%) were confirmed as having residual liver tumours within 6 months by several procedures, such as surgical resection (n=5), biopsy at the time of follow-up RFA (n=1) and other imaging modalities (contrast-enhanced CT: n=6, angiography: n=3, MRI: n=1). In these cases, however, the course of disease progression was slow and controllable because these lesions tended to respond to the subsequent repeated therapies.

Table 2 Post-therapeutic FDG PET: visual diagnosis of lesion viability and survival prediction

	Viability of hepatic lesions (based on pathological evaluation and clinical follow-up of 6months)	Viability of metastasis (based on clinical follow-up of 6months)	Survival prediction[a] (death within 12months)	Survival prediction[b] (death within 24months)
Sensitivity	62.8% (27/43 cases)	78.6% (22/28 cases)	96.0% (24/25 cases)	92.5% (37/40 cases)
Specificity	95.8% (23/24 cases)	92.3% (36/39 cases)	68.0% (17/25 cases)	100% (7/7 cases)
Positive predictive Value	96.4% (27/28 cases)	88.0% (22/25 cases)	75.0% (24/32 cases)	100% (37/37 cases)
Negative predictive Value	59.0% (23/39 cases)	85.7% (36/42 cases)	94.4% (17/18 cases)	70.0% (7/10 cases)
Accuracy	74.6% (50/67 cases)	86.6% (58/67 cases)	82.0% (41/50 cases)	93.6% (44/47 cases)

[a] Excluding patients who are alive within 12 months

[b] Excluding patients who are alive within 24 months

As for the diagnosis of viability of metastatic lesions, the sensitivity (78.6%, 22/28 cases) was higher than that of hepatic lesions. The positive predictive value in metastatic lesions (88.0%, 22/25 cases) was lower than that in hepatic lesions (96.4%, 27/28 cases). Three false-positive cases for metastatic lesions were as follows: remnant stomach after distal gastrectomy mimicking peritoneal dissemination, sarcoid nodules mimicking mediastinal lymph nodes metastases and faint thoracic vertebral uptake mimicking bone metastasis. Ultimately, the visual diagnostic accuracy of post-therapeutic lesion viability was higher in the metastatic lesions (86.6%, 58/67 cases) than that in hepatic lesions (74.6%, 50/67 cases).

Survival prediction by FDG PET

Survival prediction by visual FDG PET in unresectable HCC patients treated by non-operative therapy is also summarized in Table 2. Of 18 patients diagnosed as negative by post-therapeutic PET, 17 survived more than 12 months (negative predictive value: 94.4%). All 37 patients diagnosed as positive by post-therapeutic PET died within 24 months (positive predictive value: 100%). Survival prediction in 24 months by FDG PET was quite accurate with the value of 93.6% (44/47 cases).

Univariate analysis of each prognostic factor

Table 3 shows the results of univariate analysis of each prognostic factor in 58 patients. Clinical stage (UICC) and Milan criteria at pre-treatment evaluation did not show significant prognostic value, while those at post-PET evaluation showed statistically significant prognostic values (p=0.001–0.0001). Pathological grade of hepatitis showed significance, while that of fibrosis did not. All of the pre-therapeutic tumour markers were not significant factors. As for the post-therapeutic tumour markers, αFP (=400 ng/ml) showed significance (p=0.001). Post-therapeutic triple plus was also significant in prognostic value (p=0.005), although only six patients were positive.

FDG PET as a prognostic factor

Table 3 also shows prognostic values of FDG PET analysis before and after the non-operative therapy. The factors "post-therapeutic visual PET diagnosis (positive or negative)" and "post-therapeutic SUV=5.0" showed significance (p=0.001). In contrast, pre-therapeutic FDG PET analysis did not show any significant value.

The results of multivariate analysis of prognostic factors for overall survival in unresectable HCC patients treated by non-operative therapy are shown in Table 4. The independent prognostic factor with highest statistical value was "post-therapeutic αFP (= 400 ng/ml)" (risk ratio=0.277, p= 0.004), followed by post-therapeutic visual PET diagnosis (risk ratio=0.212, p=0.0056). On the other hand, the factor "SUV=5.0" was not significant as a predictor (risk ratio=0.889, p=0.810). "Clinical stage at post-PET evaluation (UICC stage IV)" and "Milan criteria at post-PET evaluation" also showed significant value (risk ratio=0.335 and 0.001, p=0.041 and 0.033, respectively). The other factors did not show any significance in the prediction of overall survival.

Based on the results of multivariate analysis, we classified the patients into two groups: high FDG group (diagnosed as positive at the post-therapeutic PET) and low FDG group (diagnosed as negative at the post-therapeutic PET). Figure 1a shows the survival curve of these two groups. The low FDG group showed higher survival (average survival: 607.9± 29.7 days) than the high FDG group (average survival: 327.5±40.1 days). The log-rank test showed a statistically significant difference in survival between these two groups (p<0.001). Table 5 reveals the characteristics of the two groups. Among the pre-treatment factors evaluated, UICC stage was the only significantly different one between the two groups. However, the other pre-treatment factors (age, gender, tumour differentiation, Milan criteria, target non-operative therapy, past history of therapy and pathological grade of hepatitis) were not different between the two groups. The other factors (clinical stages and Milan criteria at post-PET evaluation) showed significant differences between the two groups, but these differences were based on the PET results, where an unexpected distant metastasis was detected by post-therapeutic PET study in 13% of patients (n=9) and PET refuted the presence of a distant metastasis in 1% of patients (n=1). Therefore, clinical stages and Milan criteria at post-PET evaluation turned out to be different between the two groups as a result of FDG PET study. Pre-therapeutic tumour markers were not different in both groups. Post-therapeutic tumour markers were lower in the low FDG group because of the response to the target non-operative therapy. Although there was a significant difference in the factors of post-therapeutic FDG PET, there was no difference in the factors of pre-therapeutic PET (SUV and diagnosis). Thus, it may be said that there was no significant bias between the two groups before the target treatment.

Analysis using FDG uptake pattern

In the present study, 29 patients received pre-therapeutic FDG PET studies. According to pre- and post-therapeutic PET results, we classified these patients (n=29) into four groups by the pattern of FDG uptake as follows (Fig. 1b): low-low uptake group (L-L group) which consisted of patients who were diagnosed as negative in pre- and post-therapeutic PET studies (n=3); high-high uptake group (H-H group) which

Table 3 Univariate analysis of prognostic factors for overall survival in 58 patients

		Mean survival				Mean survival	
	n	days	*p*		*n*	days	*p*
Age (years)				Grade of fibrosis			
<60	26	438	0.76	None	3	158	0.77
≥60	32	465		Low	9	518	
Gender				Moderate	7	283	
Male	48	450	0.62	High	18	308	
Female	10	327					
Tumour differentiation							
Well	3	22	0.88	Pre-therapeutic tumour markers			
Moderately	16	487		αFP (ng/ml)			
Poorly	14	310		<400	34	489	0.12
Unknown	25	462		400 or higher	20	286	
Target therapy in the present study				αFP-L3 fraction (%)			
TACE[a]	22	498	0.13	<15	11	305	0.18
TAI[b]	26	318		15 or higher	18	287	
RFA	4	133		PIVKA-II (AU/ml)			
Systemic chemotherapy	6	339		<400	35	433	0.65
Clinical stage at pre-treatment				400 or higher	16	301	
UICC, 6th edition				Triple plus (αFP=400 or higher & αFP-L3=15 or higher & PIVKA-II=400 or higher)			
Stage II–III	42	475	0.30	Triple plus	6	317	0.76
Stage IV	16	276		Negative	44	421	
Milan criteria at pre-treatment							
Fulfilled	20	495	0.25				
Beyond	38	431		Post-therapeutic tumour markers			
Clinical stage at post-PET evaluation				αFP (ng/ml)			
UICC, 6th edition				<400	39	516	0.001[c]
Stage II–III	36	532	0.001[c]	400 or higher	19	262	
Stage IV	22	259		αFP-L3 fraction (%)			
Milan criteria at post-PET evaluation				<15	32	488	0.16
Fulfilled	17	all alive	0.0001[c]	15 or higher	23	302	
Beyond	41	376		PIVKA-II (AU/ml)			
Past history of therapy				<400	37	481	0.11
Partial resection ±	29/29	398/502	0.13	400 or higher	17	389	
LDLT ±	1/57	-		Triple plus (αFP=400 or higher & αFP-L3=15 or higher & PIVKA-II=400 or higher)			
TACE ±	43/15	458/290	0.90	Triple plus	6	218	0.005[c]
TAI ±	31/27	445/452	0.98	Negative	46	474	
RFA ±	28/30	317/471	0.88	Pre-therapeutic FDG PET			
PEIT ±	12/46	167/457	0.84	Visual PET diagnosis			
Child-Pugh classification at PET study				Positive	18	294	0.78
A	33	438	0.0001[c]	Negative	11	399	
B	22	322		SUV			
C	3	84		<5.0	15	419	0.73
Aetiology of hepatitis				5.0 or higher	13	278	
HBV	15	421	0.14	Post-therapeutic FDG PET			
HCV	37	490		Visual PET diagnosis			
Others	6	142		Positive	32	327	0.0001[c]
Pathological grade of hepatitis				Negative	26	608	
None	2	-	0.01[c]	SUV			
Low	22	487		<5.0	40	523	0.0001[c]
Moderate	12	268		5.0 or higher	18	227	
High	1	131					

αFP alpha-fetoprotein, *αFP-L3* lens culinaris agglutinin-reactive fraction of αFP, *PIVKA-II* protein induced by vitamin K absence or antagonist II, *FDG* fluorodeoxyglucose, *SUV* standardized uptake value

[a] Including PEIT

[b] Including overlapping therapy

[c] Significant by log-rank test